



Contents lists available at ScienceDirect

European Journal of Medicinal Chemistry

journal homepage: <http://www.elsevier.com/locate/ejmech>

Research paper

Novel bis-arylalkylamines as myeloperoxidase inhibitors: Design, synthesis, and structure-activity relationship study



Iyas Aldib^a, Michel Gelbcke^a, Jalal Soubhye^a, Martine Prévost^e, Paul G. Furtmüller^c, Christian Obinger^c, Betina Elfving^d, Ibaa Chikh Alard^f, Goedele Roos^e, Cédric Delporte^{a,b}, Gilles Berger^a, Damien Dufour^{a,b}, Karim Zouaoui Boudjeltia^g, Jean Nève^{a,b}, Francois Dufrasne^a, Pierre Van Antwerpen^{a,b,*}

^a Laboratoire de Chimie Pharmaceutique Organique, Faculté de Pharmacie, Université Libre de Bruxelles, Brussels, Belgium

^b Analytical Platform of the Faculty of Pharmacy, Université Libre de Bruxelles, Brussels, Belgium

^c Department of Chemistry, Division of Biochemistry at the Vienna Institute of Biotechnology, BOKU—University of Natural Resources and Life Sciences, Muthgasse 18, A-1190, Vienna, Austria

^d Translational Neuropsychiatry Unit, Department of Clinical Medicine, Aarhus University, Aarhus, Denmark

^e Laboratoire de Structure et Fonction des Membranes Biologiques, Université Libre de Bruxelles, Brussels, Belgium

^f Laboratoire de Pharmacie Galénique et de Biopharmacie, Faculté de Pharmacie, Université Libre de Bruxelles (ULB), Brussels, Belgium

^g Laboratory of Experimental Medicine, A. Vésale Hospital, Faculty of Medicine, Université Libre de Bruxelles, Montigny-le-Tilleul, Belgium

ARTICLE INFO

Article history:

Received 13 May 2016

Received in revised form

5 July 2016

Accepted 22 July 2016

Available online 25 July 2016

Keywords:

Myeloperoxidase selective inhibitors

Bis-arylalkylamines derivatives

Reversible inhibitors

SERT

Pharmacomodulation

Docking

ABSTRACT

Human myeloperoxidase (MPO) plays an important role in innate immunity but also aggravates tissue damage by oxidation of biomolecules at sites of inflammation. As a result from a recent high-throughput virtual screening approach for MPO inhibitors, bis-2,2'-[(dihydro-1,3(2*H*,4*H*) pyrimidinediyl)bis(-methylene)]phenol was detected as a promising lead compound for inhibition of the MPO-typical two-electron oxidation of chloride to hypochlorous acid ($IC_{50} = 0.5 \mu M$). In the present pharmacomodulation study, 37 derivatives of this lead compound were designed and synthesized driven by comprehensive docking studies and the impact on the chlorination activity of MPO. We describe the structural requirements for optimum (i) binding to the heme periphery and (ii) inhibition capacity. Finally, the best three inhibitors (bis-arylalkylamine derivatives) were probed for interaction with the MPO redox intermediates Compound I and Compound II. Determined apparent bimolecular rate constants together with determination of reduction potential and nucleophilicity of the selected compounds allowed us to propose a mechanism of inhibition. The best inhibitor was found to promote the accumulation of inactive form of MPO-Compound II and has $IC_{50} = 54 \text{ nM}$, demonstrating the successful approach of the drug design. Due to the similarity of ligand interactions between MPO and serotonin transporter, the selectivity of this inhibitor was also tested on the serotonin transporter providing a selectivity index of 14 ($KiSERT/IC_{50}MPO$).

© 2016 Elsevier Masson SAS. All rights reserved.

Abbreviations: MPO, myeloperoxidase; HDL, high density lipoprotein; LDL, low density lipoprotein; NSAIDs, nonsteroidal anti-inflammatory drugs; SHA, salicylhydroxamic acid; SERT, serotonin transporter; HTVS, high throughput virtual screening; DMSO, dimethyl sulfoxide; TEA, trimethylamine; E° , standard reduction potential; E' , reduction potential; NHE, normal hydrogen electrode; RT, room temperature; DCM, dichloromethane; EtOAc, ethyl acetate.

* Corresponding author. Laboratoire de Chimie Pharmaceutique Organique, Faculté de Pharmacie, Université Libre de Bruxelles, Brussels, Belgium.

E-mail address: pvantwer@ulb.ac.be (P. Van Antwerpen).

1. Introduction

Myeloperoxidase (MPO, EC 1.11.2.2) is a heme enzyme belonging to Family 1 of the peroxidase-cyclooxygenase superfamily [1]. It is expressed mainly in human neutrophils and to some extent in monocytes [2–6] and activates hydrogen peroxide to oxidize a great variety of organic substrates to free radicals. However, what sets MPO apart from other mammalian heme proteins is its exceptional ability to oxidize chloride to hypochlorous acid, a strong oxidant that kills bacteria and is toxic to human cells. So far MPO is the only known heme protein with three heme to protein

covalent linkages (two ester bonds and one electron withdrawing sulfonium ester linkage). These posttranslational modifications distort the prosthetic group from planarity and lend an extraordinary one- and two-electron oxidation capacity to the relevant redox intermediate Compound I [7–9].

Neutrophils are innate immune cells that contain granules loaded with antimicrobial peptides and proteins including MPO. When neutrophils encounter pathogenic bacteria, they trap them within intracellular vacuoles called phagosomes, into which they discharge their granule contents. Simultaneously dioxygen is reduced to superoxide that dismutates and delivers hydrogen peroxide for the initiation of MPO activity and, finally, the production of antimicrobial hypochlorous acid/hypochlorite (HOCl/ClO^-) [10–14]. Myeloperoxidase may also kill bacteria outside of neutrophils. Phagocytic and inflammatory stimuli induce neutrophils to cast out web-like structures consisting of DNA, histones and granule proteins including MPO. These neutrophil extracellular traps (NETS) also contribute to trapping and killing bacteria [15].

However, interest in MPO exploded when it was found to aggravate tissue damage by oxidation of lipids, (lipo)proteins or DNA at sites of inflammation [16–18]. It has been reported that MPO plays a role in ischemia, and neurodegenerative diseases such as multiple sclerosis and Parkinson disease [17,19–24], as well as in sepsis [25], lung disease [26], atherosclerosis [27] and atrial fibrillation [28]. For example, in cardiovascular diseases MPO mediates the production of proatherogenic lipoproteins (oxidized LDL and HDL) promoting endothelial dysfunction, atheroma plaque formation, thrombosis, and ventricular remodeling [29,30]. The MPO/ $\text{H}_2\text{O}_2/\text{Cl}^-$ system seems to be involved in initiation and propagation of inflammation during the development of atherosclerotic lesion [31]. Indeed, Mox-LDL (LDL oxidized by MPO) has been shown to initiate inflammatory responses in monocytes and endothelial cells [32]. Myeloperoxidase takes also a part in transforming high-density lipoprotein (HDL) by the selective modification of apolipoprotein A-1 to dysfunctional HDL [32–34].

Consequently, blocking the activity of MPO is a potential pharmacological strategy for prevention and treatment of a broad range of inflammatory diseases [35]. In the beginning upon random chemical screening several natural compounds and commercial drugs with antioxidant, anti-inflammatory and antihistaminic activity were shown to inhibit MPO activity, including flufenamic acid and indomethacin [36], nonsteroidal anti-inflammatory drugs (NSAIDs) [37], e.g. diclofenac [38], flavonoids and polyphenols [39], chalcones [40–42], resveratrol [43], caffeic acid, ferulic acid and gallic acid [44]. Furthermore, indole and tryptamine derivatives carrying an amine or an amide group on the carbon side chain connected to the indole ring [45–47], salicylhydroxamic acid (SHA) and hydrazide derivatives [48], isoniazide [49], dapsone [50], thioxanthine derivatives [51], aromatic hydroxamates derivatives [52] and indazolone analogs [53] were demonstrated to block MPO activity.

Certainly, random screening was a very important step in the process of discovering MPO inhibitors. But more recently, high throughput virtual screening (HTVS) could be applied since high resolution crystal structures of human MPO and MPO complexes became available [54–57]. The first HTVS for MPO inhibitors based on the interactions of SHA with active site residues was performed in 2011 resulting in the selection of nine benzoic acid hydrazide derivatives from Zinc database. The activity of those selected compounds did not exceed that from SHA [58]. Finally, Aldib et al. [32] uncovered eight novel and different (positively charged) scaffolds of potential MPO inhibitors which were predicted to bind close to Glu102 at the active site of MPO. The best inhibitors were: **A1**, bis-2,2'-[(dihydro-1,3(2*H*,4*H*)-pyrimidinediyl)bis(methylene)]phenol, and **F9**, 8-[(2-aminoethyl)amino]-3,7-dihydro-3-methyl-7-

(3-phenoxypropyl)-1*H*-purine-2,6-dione (Fig. 1). The latter is a xanthine structure which is related to the thioxanthine derivatives developed by AstraZeneca [59], while the hexahydropyrimidine structure was a novel chemical scaffold [32].

The purpose of the present study was to use the hexahydropyrimidine structure as a basis for pharmacomodulation in order to improve the potency in MPO inhibition. We first describe (i) the strategy of design driven by comprehensive docking studies, (ii) the chemical synthesis of these compounds as well as (iii) their impact on the chlorination activity of MPO. Finally, we propose a mechanism of inhibition based on these observations in combination with multi-mixing stopped-flow spectroscopic studies.

2. Results

2.1. Docking experiments

Based on HTVS bis-2,2'-[(dihydro-1,3(2*H*,4*H*)-pyrimidinediyl)bis(methylene)]phenol (**A1**) (Fig. 1) was selected as a lead compound as it was demonstrated to inhibit the chlorinating activity of MPO ($\text{IC}_{50} = 0.5 \mu\text{M}$) [32]. The X-ray structures of human MPO in complex with cyanide and thiocyanate (PDB code 1DNW) as well as in complex with **HX1** (PDB code 4C1M) were used as target structures in the docking studies.

The reliability of our docking procedure was previously assessed by comparing the docking of **SHA** with its position in the crystal structure of the MPO complex [61]. We validated further this procedure by docking 2-(3,5-bistrifluoromethylbenzylamino)-6-oxo-1*H*-pyrimidine-5-carboxylic acid (**HX1**) (Fig. 1) in the X-ray structure of the complex (PDB ID: 4C1M) [52,60] and as well as in the other target X-ray structure (PDB ID: 1DNW). The best pose of **HX1** in 4C1M, as determined by its lowest root-mean square deviation computed on all heavy atoms (RMSD) of 0.39 Å, is very similar to its crystal position. (Fig. 2A–B). **HX1** forms several non-covalent interactions: a π -stacking with pyrrole ring D and hydrogen bonds to Arg239, Gln91 and His95 with the ketone group of its pyrimidin-(*H*)-one ring, its amide carbonyl and hydroxyl group of the hydroxamic function, respectively. A stacking similar to that observed for **HX1** is also found in the crystal structure of **SHA**-MPO complex [60] as well as in its docked position (Fig. 2D) in addition to hydrogen bonds formed with Arg239, Gln91 and His95. Similar stacking positions with pyrrole ring D were also observed in docked positions of 5-fluorotryptamine and 3-(aminoalkyl)-5-fluoroindole derivatives [45,46,61]. The poses of **HX1** in 1DNW (Fig. 2C) are less similar as indicated by a RMSD of 4.1 Å. However, this higher RMSD value is mainly attributed to the bistrifluoromethylbenzyl moiety as shown by a RMSD of 0.7 Å calculated by removing this group. The differences observed in both target structures could be attributed to the better structural complementarity between the MPO conformation and **HX1** in the 4C1M structure. In any case, these docking data clearly underline that the applied docking procedure provides a good basis for the planned pharmacomodulation study.

Next we probed docking of **A1** [32] (Fig. 2) to the two target structures (Fig. 2E–F). In both cases, **A1** shows almost the same poses. In detail, the best-score position of **A1** features a π -stacking of one phenol ring (ring A) of **A1** with the pyrrole ring D as well as formation of a H-bond between the OH-group of this phenol ring and Arg239. Furthermore, an ionic interaction between Glu102 and the positively charged nitrogen of **A1** is established in addition to H-bonding between Glu102 and Phe147 with the OH-group of the other phenol ring.

Based on the observed binding modes of **A1** (Fig. 2), different approaches were developed for the design of derivatives. In the modulation process we focused mainly on the substitution of the

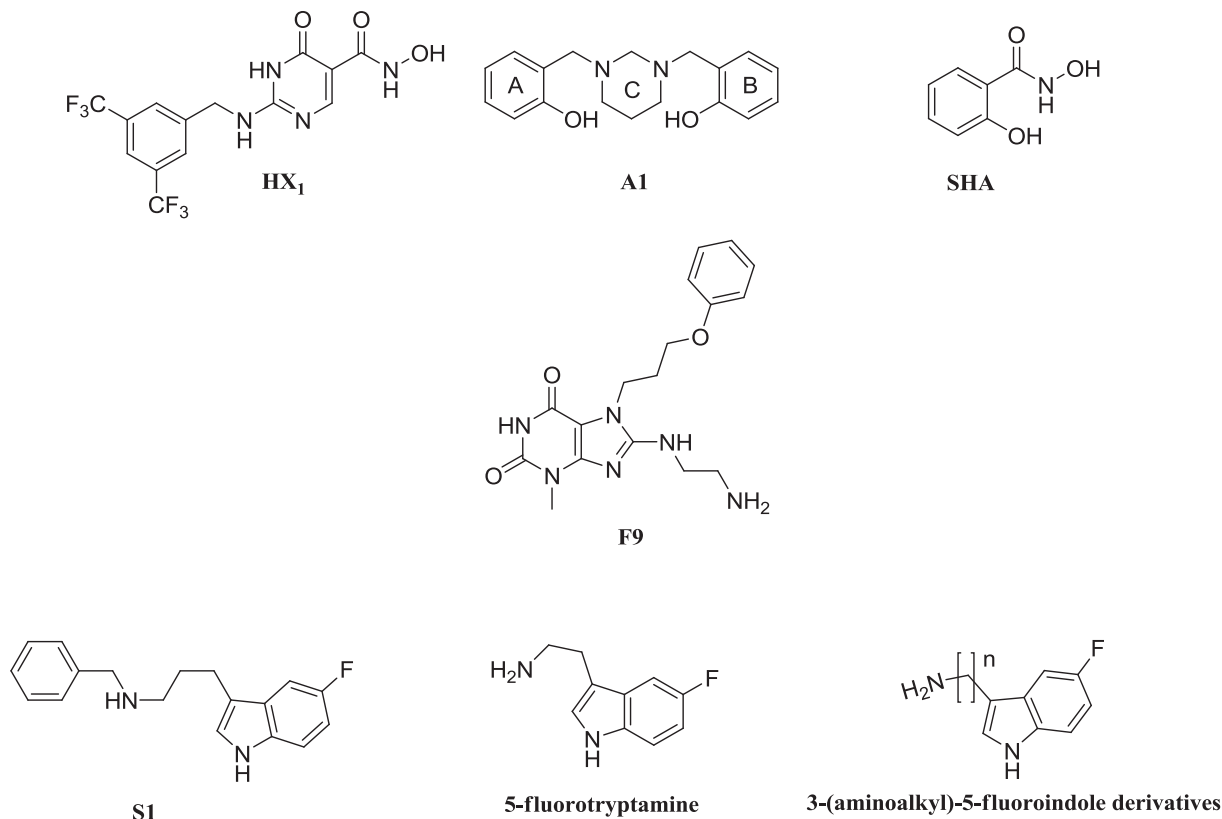


Fig. 1. Structures of A1, HX1, SHA, S1, 5-fluorotryptamine, 3-(aminoalkyl)-5-fluoroindole derivatives and F9.

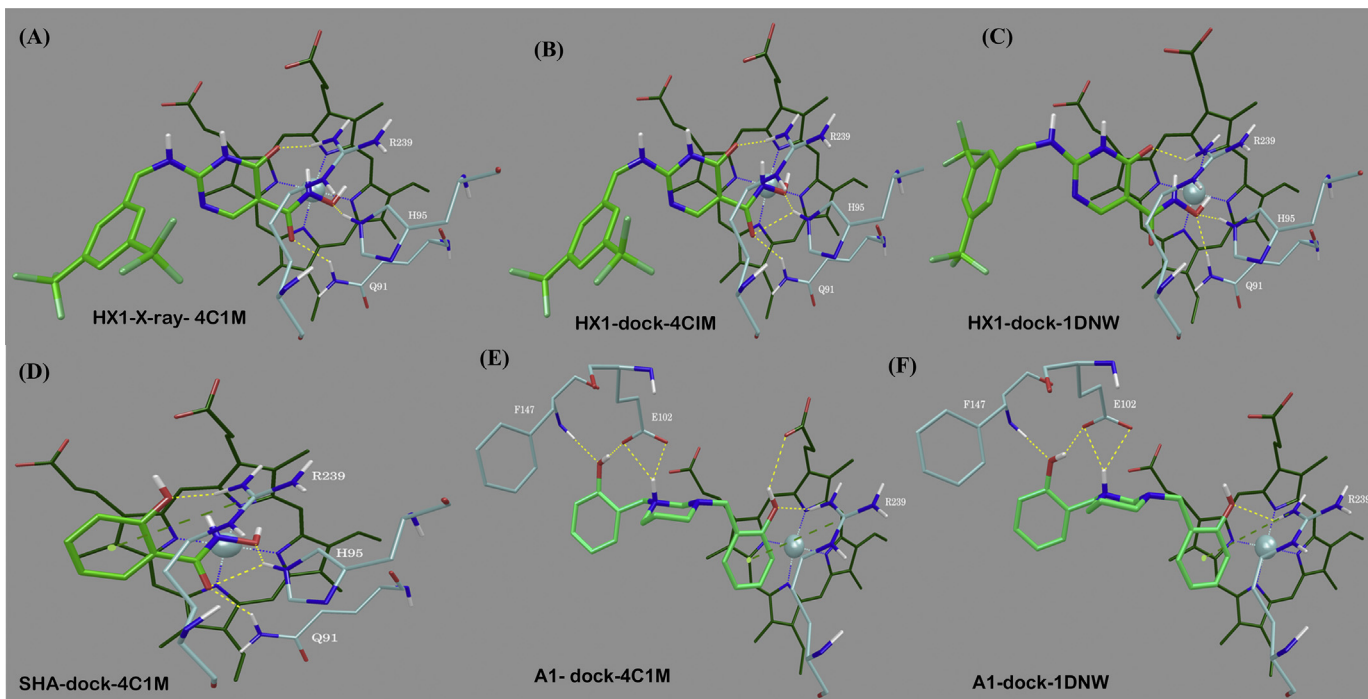


Fig. 2. Positions of HX1, SHA and A1 in MPO structures. (A) X-ray structure of human MPO in complex with HX1 (PDB ID: 4C1M). (B) Docked pose of HX1 in the X-ray MPO structure (PDB ID: 4C1M). (C) Docked pose of HX1 in the X-ray MPO structure (PDB ID: 1DNW). (D) Docked pose of SHA in the X-ray MPO structure (PDB ID: 4C1M). (E) Docking pose of A1 in the X-ray MPO structure (PDB ID: 4C1M). (F) Docking pose of A1 in the X-ray MPO structure (PDB ID: 1DNW). Hydrogen bonds, cation- π and π - π interactions are depicted as yellow, green and blue dotted lines. The ligands are shown as thick lines and the interacting residues as well as the heme as thinner lines. (For interpretation of the references to colour in this figure legend, the reader is referred to the web version of this article.)

aromatic rings A and B. All designed compounds were docked in the two target structures. For the sake of simplicity, only the poses obtained in 4C1M are described unless otherwise specified. In most cases the docked poses are similar for both targets. Fig. 2.

2.1.1. The role of hydroxyl groups on aromatic rings A and B

Upon elimination of the hydroxyl groups on rings A and B of **A1** (Fig. 1) compound **2** was designed and docked to both MPO receptor structures. Compared to **A1** (−8.1 kcal/mol in 4C1M) the calculated free energy upon binding of the best pose decreases to −5.4 kcal/mol. In 4C1M, in addition to an aromatic stacking with the pyrrole, the observed interactions between the ligand and the protein are a cation- π with Arg239, π - π interaction with His95 and an ionic bond between Glu102 and the tertiary amine in ring C. (Table 2 and Supplementary materials).

Introduction of a ketone function on the methylene group of ring C in compound **2** aiming at increasing its stability toward hydrolysis [62], i.e. compound **3**, results in a docked pose featuring a stacking with the pyrrole and one cation- π with Arg239 as in compound **2**. No H-bonds are observed (Table 2 and Supplementary materials).

2.1.2. Shifting the position of the amino groups in ring C and introduction of fluorine

Changing the positions of amino groups in compound **A1** through replacing hexahydropyrimidine ring by piperazine ring should increase the hydrolytic stability [62,63] and leads to a decrease in the predicted binding energy. Interactions formed by compound **4** are roughly similar to those of **A1** except for the hydroxyl group of the ring that is not stacked onto the pyrrole and which lacks hydrogen bonds (Table 2 and Supplementary materials).

Further modification of compound **4** was achieved by substitution of the OH-function in rings A and B by fluorine (compound **5**) or elimination of the OH-group and introduction of fluorine at different positions (compounds **6** and **7**) or elimination of both OH-groups (compound **8**) (Table 1). Fluorine is often used to substitute OH-groups since it can also establish polar interactions and in addition increases the metabolic stability of molecules [64]. Introduction of fluorine substituents slightly decreases the predicted affinity of the ligands. Generally, for compounds **5–8**, Glu102 and Arg239 with **A1** establish an ionic interaction and a cation- π interaction respectively but no hydrogen bonds are observed. (Table 2 and Supplementary materials).

2.1.3. Elimination of ring B and of an amino group in ring C

Compounds **9** and **10** lack both the aromatic ring B as well as one of the tertiary amino groups of ring C to study the role of ring A and one amino group (Table 1). Compound **9** (with smaller distance between OH and amino group) and **10** both show a stacking though shifted for compound **9** and exhibit a substantial decrease in the predicted affinity relative to **A1**. They formed interactions similar to **A1** apart from those arising from the second hydroxylated ring (see Table 2 and Supplementary materials).

2.1.4. Opening heterocycle C

This modulation was done in order to test the effect of removal of the heterocycle C. However, the amine function was kept as it was demonstrated to be beneficial for inhibition of MPO [45,47]. Next we probed the length of the bridge between this amino group and aromatic ring B as well as the impact of substitutions on rings A and B (Table 1). With increasing lengths of the bridge both the lipophilicity and the flexibility of the ligand could be raised. In compounds **11** and **12**, the benzyl moiety makes a T-shaped interaction with or shifted stacking on pyrrole D while the hydroxyl

Table 1

List of all synthesized compounds including IC₅₀ values (μ M) values and standard reduction potentials, E^o (mV). N.A., no activity; N.D., no data available. N.I.R., not in range, i.e. >1.2 V.

Compound	R	X	IC ₅₀	E ^o
A1	OH	CH ₂	0.5 ± 0.1	N.D
2	H	CH ₂	N.A	N.I.R
3	H	C=O	N.A	N.I.R

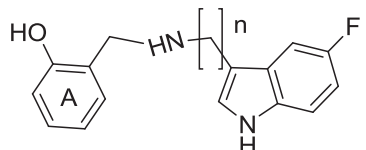
Compound	R ₁	R ₂	R ₃	IC ₅₀	E ^o
4	OH	H	H	1.4 ± 0.2	1072
5	F	H	H	>10	1100
6	H	F	H	>10	1062
7	H	H	F	>10	1017
8	H	H	H	>10	996

Compound	X	Y	IC ₅₀	E ^o
9	N	CH ₂	>10	953
10	CH	NH	>10	960

Compound	R ₁	R ₂	R ₃	R ₄	n	IC ₅₀	E ^o
11	OH	H	H	H	2	0.7 ± 0.1	973
12	OH	H	H	H	3	1.2 ± 0.6	928
13	H	H	H	H	2	N.A.	N.I.R.
14	H	H	H	H	3	N.A.	N.I.R.
15	OH	H	H	F	2	0.67 ± 0.16	948
16	OH	H	H	F	3	0.37 ± 0.06	902
17	OH	H	H	OCH ₃	2	1.85 ± 0.01	907
18	OH	H	H	OH	2	0.65 ± 0.02	870
19	OH	H	H	OCH ₃	3	2.5 ± 0.8	871
20	OH	H	H	OH	3	0.35 ± 0.05	844
21	H	H	H	OCH ₃	2	N.A.	N.I.R.
22	H	H	H	OH	2	2.70 ± 0.01	897
23	H	H	H	OCH ₃	3	N.A.	N.I.R.
24	H	H	H	OH	3	0.36 ± 0.11	825
25	F	H	H	OCH ₃	2	N.A.	N.I.R.
26	F	H	H	OH	2	0.70 ± 0.06	856
27	F	H	H	OCH ₃	3	N.A.	N.I.R.
28	F	H	H	OH	3	0.27 ± 0.03	833
29	H	H	F	OCH ₃	2	N.A.	N.I.R.
30	H	H	F	OH	2	1.16 ± 0.05	865
31	H	H	F	OCH ₃	3	N.A.	N.I.R.
32	H	H	F	OH	3	0.49 ± 0.12	869
33	H	F	H	OCH ₃	2	N.A.	N.I.R.
34	H	F	H	OH	2	0.66 ± 0.17	807
35	H	F	H	OCH ₃	3	N.A.	N.I.R.
36	H	F	H	OH	3	0.37 ± 0.05	820

(continued on next page)

Table 1 (continued)



Compound	n	IC ₅₀	E ^{o†}
37	2	0.085 ± 0.017	902
38	3	0.054 ± 0.007	872

group kept on aromatic ring A and the amine groups makes interactions similar to those of **A1** (Table 2 and Supplementary materials). Upon elimination of the hydroxyl group (i.e. compounds **13** and **14**) these hydrogen bonds are lost and the affinity scores are decreased by about 1.5 kcal mol⁻¹ compared to compounds **11** and **12** (Table 2). A cation- π interaction is however formed with the aromatic moiety stacked on pyrrole D and Arg239.

Keeping one hydroxyl group on aromatic ring A and replacing the other one on aromatic ring B by fluorine together with either an ethyl or propyl bridge lead to compounds **15** and **16** (Table 1). Their docking poses show stacking or shifted stacking poses of the fluorobenzyl group on pyrrole D and an ionic interaction with Glu102 (Table 2). Keeping the hydroxyl group on aromatic ring A and having on ring B the OH-group or a methoxy group together with either an ethyl or propyl bridge give compounds **17–20** (Table 2, Fig. 3A). Compounds **17** and **19** (carrying the methoxy group) feature a slightly more favorable free energy of binding relative to the compounds carrying an -OH-group (Table 2).

Removing the hydroxyl group on aromatic ring A and keeping either a hydroxyl or methoxy group on ring B together with either an ethyl or propyl bridge lead to compounds **21–24** (Table 1). In contrast to compounds **21** and **23** (carrying the methoxy group), compounds **22** and **24** feature a better stacking onto pyrrole D and have their -OH-groups hydrogen bonding to Arg239 (Table 2 Supplementary materials).

Further modulation included (i) replacement of the hydroxyl group on aromatic ring A by fluorine in *ortho* (R₁), *meta* (R₂) or *para* (R₃) positions, (ii) having either a hydroxyl or methoxy group (R₄) on aromatic ring B, and (iii) using ethyl or propyl as bridge (compounds **25–36**, Table 1). Docking experiments show that all compounds carrying a hydroxyl group on ring B feature their fluorobenzyl moieties stacked onto the pyrrole D whereas in compounds carrying the stacking onto the heme is provided either by the a methoxy- or the fluorobenzyl group. Compared to **A1** the predicted affinities are lower for all compounds (Table 2).

The last two compounds **37** and **38** were designed by hybridization of the hit **A1** and 5-fluorotryptamine where hydroxyl group in aromatic ring A (from **A1**) is linked to 5-fluoroindole (from 5-fluorotryptamine), using ethyl or propyl as linker (Table 1). Both compounds exhibit an ionic interaction with Glu102 and hydrogen bonds with Phe147 and Glu102 and a cation- π with Arg239. Remarkably the predicted affinity of compound **37** is as high as for **A1** (Table 2).

To sum up all designed compounds have in common to form an ionic interaction between Glu102 and their amine group and a

stacking of one of their aromatic moiety on pyrrole D. A cation- π makes with Arg239 is also a rather recurrent interaction. Although it is always perilous to rank the ligand affinity using the scoring functions one can however notice that compound **38** is the compound predicted to have the best score.

2.2. Chemistry

Schemes 1–4 summarize the procedures for syntheses of compounds **1–38**. Synthesis of the hexahydropyrimidine derivative **2** was based on a reductive amination reaction [65,66] followed by a condensation reaction with formaldehyde. For synthesis of compound **3** different reaction conditions [67] were chosen (Scheme 1). For synthesis of piperazine [68] derivatives different aldehydes (compounds **4–7**) or benzylchloride [69] (compound **8**) were used (Scheme 2). The piperidine derivative **9** was synthesized by same method used for piperazine derivatives, while other piperidine derivative **10** was obtained by demethylation of 3-(2-methoxybenzyl)piperidine [70,71] (Scheme 3). The pathways followed for the syntheses of bis(arylalkyl)amine derivatives (compounds **11–36**) and the indole derivatives (**37, 38**) are summarized in Scheme 4. They include either a reductive amination step or two steps consisting of a reductive amination followed by a demethylation reaction [65,66,70,71] (Scheme 4).

2.3. Inhibition of chlorination activity of myeloperoxidase

For assessment of inhibition of the chlorination activity of MPO (i.e. the production of hypochlorous acid) the taurine chloramine assay was used in a high-throughput screening mode. Table 1 presents the respective IC₅₀ values for the 37 synthesized compounds. The IC₅₀ value for the lead compound **A1** was 500 nM. The data clearly underline the importance of the hydroxyl groups on the aromatic rings A and B for inhibition of taurine chlorination. Except compound **4** all piperazine derivatives without a hydroxyl group (i.e. compounds **5–8**) were poor inhibitors. This was also the case for compounds **9** and **10** that lack one of the two aromatic rings.

By contrast the best inhibitors were those with 5-fluoroindole instead of aromatic ring B with IC₅₀ values of 85 nM (compound **37**) and 54 nM (compound **38**), respectively. The latter has the longer (propyl) bridge between the amino function and the indole ring. Further compounds with IC₅₀ values lower than **A1** include propylamine compounds (**16, 20, 24, 28, 32, and 36**). Importantly, their longer bridge (propyl) chain gives more flexibility between the amino group and the aromatic ring B. They have also a fluorine (compound **16**) or hydroxyl group (compounds **20, 24, 28, 32, and 36**) at position R₄ on aromatic ring B. As demonstrated in Table 1 compounds that have a methoxy group at position R₄ on the aromatic ring B and fluorine on aromatic ring A or compounds which have no hydroxyl groups on two rings A, B were unable to block the chlorination activity of MPO as with **13, 14, 21, 23, 25, 27, 29, 31, 33, and 35**. Furthermore the position of fluorine on aromatic ring A seems to modulate the inhibition capacity of those compounds to some extent with compound **28** (*ortho* position) being the most effective of this series. Note that exchange of the hydroxyl group (*ortho* position) on aromatic ring A (**18, 20**) by fluorine (**26, 28**) decreases the respective IC₅₀ values (Table 1). Some ethylamine derivatives (compounds **11, 15, 17, 18, 22, 26, 30, and 34**) and propylamine derivatives (only hydroxyl on ring A or one methoxy on ring B and one hydroxyl on A as **12, 19**) also showed reasonable inhibition of MPO-mediated halogenation of taurine but their respective IC₅₀ values were higher than that of the **A1**.

Table 2

List of all compounds along with the predicted affinity (ΔG_{score} (kcal/mol)) of their best score docked positions and their interactions made with the receptor structure (PDB code: 4C1M). HB, hydrogen bonds; SB, ionic interaction or salt bridge; Cat- π , cation- π ; π - π , interaction π - π ; Stacking, stacking with one heme pyrrole, (S, full stacking; SS, shifted stacking, TS, T-shaped interaction).

Compound	Receptor 4C1M					
	ΔG_{score}	Compound-receptor interactions				
		HB	SB	Cat- π	π - π	Stacking
HX ₁	-6.4	Gln91 His95 Arg239	–			S
A ₁	-8.1	Arg239 Glu102 Phe147 Heme propionate	Glu102	Arg239		S
2	-5.4	–	Glu102	Arg239	His95	S
3	-4.1	–	–	Arg239		S
4	-6.6	Arg239 Heme propionate	Glu102	Arg239		S
5	-5.2	–	Glu102	Arg239		SS
6	-5.7	–	Glu102	Arg239 Arg424		S
7	-4.8	–	Glu102	Arg239		S
8	-5.3	–	Glu102	Arg239		S
9	-4.4	Heme propionate	Glu102	Arg239		SS
10	-5.6	Arg239 Heme propionate	Glu102	Arg239		S
11	-6.3	Glu102 Phe147	Glu102			SS
12	-6.9	Glu102 Phe147	Glu102			TS
13	-4.9	–	Glu102	Arg239		S
14	-5.3	–	Glu102	Arg239		S
15	-6.0	Phe147 Glu102	Glu102			SS
16	-5.4	Heme propionate	Glu102	Arg239	His95	S
17	-7.6	Glu102 Phe147	Glu102			SS
18	-6.5	Heme propionate	Glu102 Heme propionate	Arg239		SS
19	-7.2	Arg239 Heme propionate	Glu102	Arg239	His95	S
20	-6.3	Heme propionate	Glu102	Arg239		SS
21	-5.8	–	Glu102 Heme propionate		Phe147	SS
22	-6.0	Arg239 Heme propionate	Glu102	Arg239 Arg424		S
23	-5.7	–	Glu102 Heme propionate	Arg239		SS
24	-5.9	Arg239	Glu102	Arg424		S
25	-5.9	–	Glu102 Heme propionate			SS
26	-5.7	Glu102 Phe147	Glu102	Arg239		SS
27	-5.8	–	Glu102 Heme propionate	Arg239	His95	S
28	-5.9	Pro145	Glu102 Heme propionate	Arg239		S
29	-5.2	–	Glu102			SS
30	-5.9	Glu102 Phe147	Glu102	Arg239		SS
31	-5.1	Arg239	Glu102	Arg239		S
32	-5.8	Pro145	Glu102 Heme propionate	Arg239		SS
33	-5.4	Arg239	Glu102	Arg239		SS
34	-5.9	Heme propionate	Glu102	Arg239		SS
35	-6.5	Arg239	Glu102	Arg239		S
36	-5.9	Pro145	Glu102 Heme propionate			SS
37	-6.2	Glu102 Phe147 Heme propionate	Glu102	Arg239		S
38	-8.3	Glu102 Phe147 Arg239 Heme propionate	Glu102	Arg239	His95	S

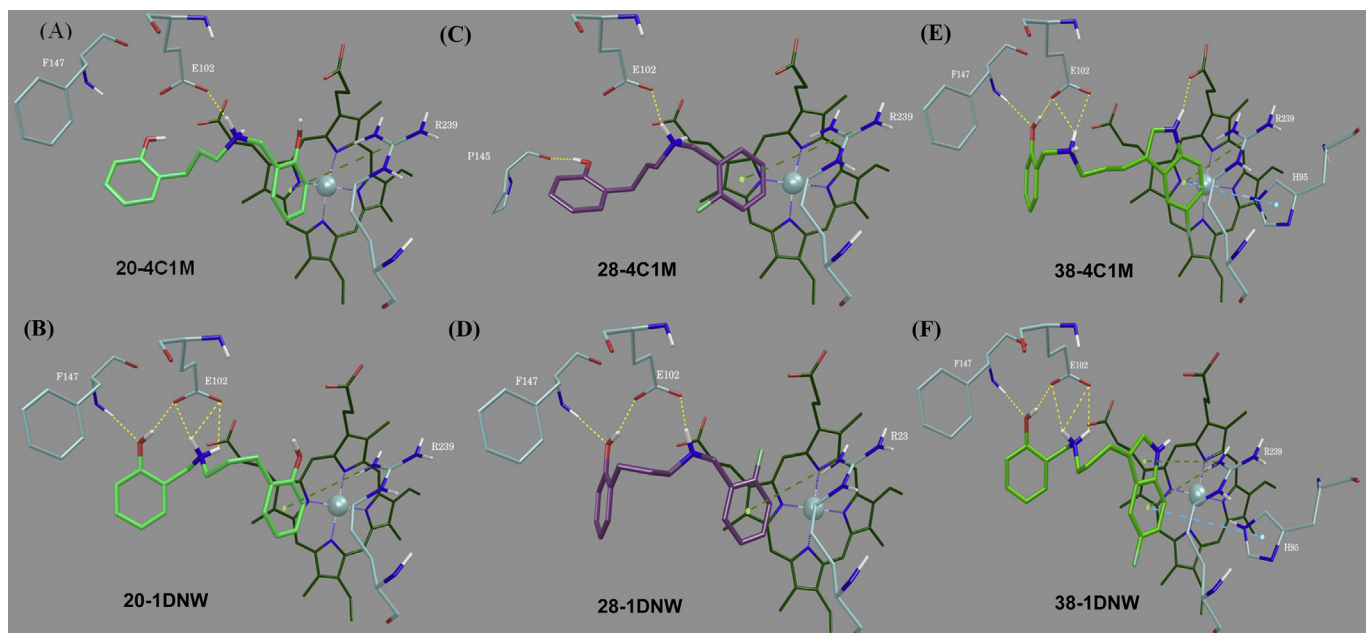
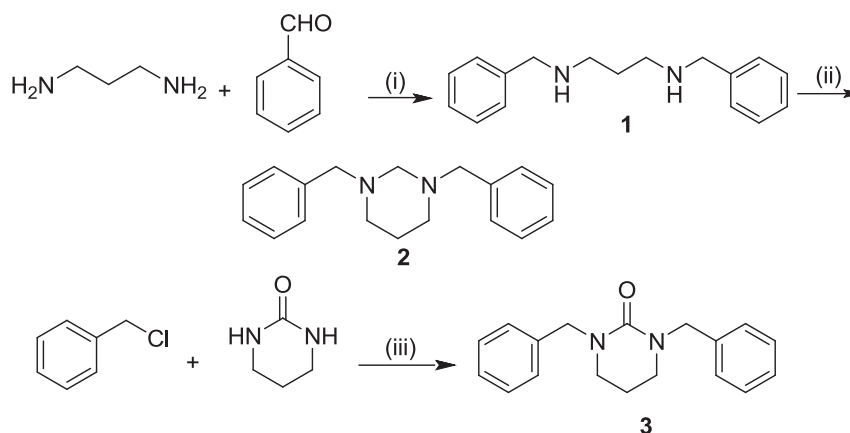


Fig. 3. Docked poses of compounds **20**, **28**, **38** in the Xray MPO structures. (A) Pose of compound **20** in the Xray MPO structure (PDB ID: 4C1M). (B) Pose of compound **20** in the Xray MPO structure (PDB ID: 1DNW). (C) Pose of compound **28** in the Xray MPO structure (PDB ID: 4C1M). (D) Pose of compound **28** in the Xray MPO structure (PDB ID: 1DNW). (E) Pose of compound **38** in the Xray MPO structure (PDB ID: 4C1M). (F) Pose of compound **38** in the Xray MPO structure (PDB ID: 1DNW). Hydrogen bonds, cation- π and π - π interactions are depicted as yellow, green and blue dotted lines. The ligands are shown as thick lines and the interacting residues as well as the heme as thinner lines. (For interpretation of the references to colour in this figure legend, the reader is referred to the web version of this article.)



Reagents and conditions

(i) NaBH_3CN , EtOH

(ii) Formaldehyde (37 wt % aqueous solution), EtOH

(iii) BnCl , NaH, Dioxane, Reflux

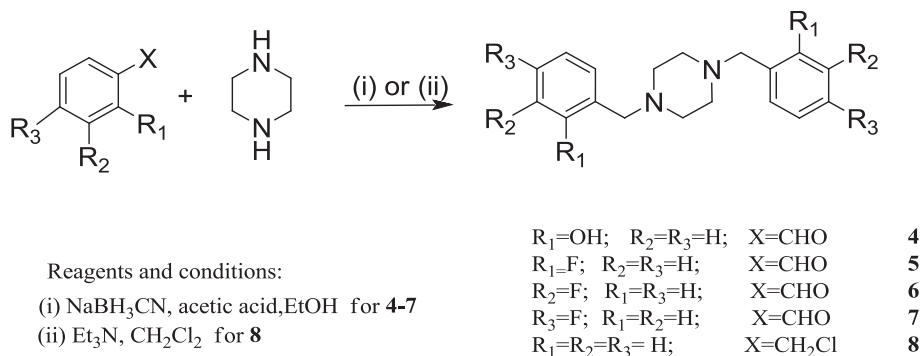
Scheme 1. Synthesis of N-N'-1,3-bisbenzyl-1,2,3,4,5,6 hexahydropyrimidine and 1,3-dibenzyl-3,4,5,6-Tetrahydro-2(1H)-Pyrimidinone.

2.4. Transient-state kinetics of the reaction between MPO Compound I and Compound II with inhibitors

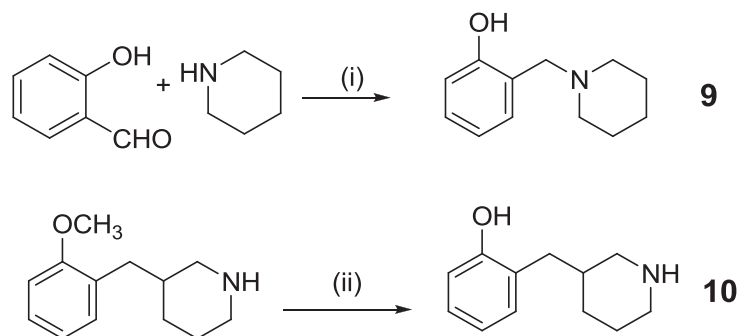
Next, the best inhibitors of MPO-mediated taurine chlorination, i.e. compounds **20**, **28** and **38** (see their docked poses in Fig. 3) were subjected to a transient-state kinetic study using multimixing stopped-flow spectroscopy [72]. Fig. 4 schematically represents the halogenation and the peroxidase cycle of MPO. For initiation of both pathways ferric MPO has to be oxidized by hydrogen peroxide to Compound I. In the halogenation cycle Compound I oxidizes halides to the corresponding hypohalous acids thereby being directly reduced to ferric MPO. In the peroxidase cycle one-electron donors

reduce Compound I in two one-electron reduction steps via Compound II to ferric MPO. Compound II is unable to oxidize halides (see Fig. 4).

For elucidation of the mechanism of MPO inhibition it is important to know the mode of interaction of these molecules with MPO Compounds I and II. Thus we performed these redox intermediates in a sequential stopped-flow mode and probed their reactivity towards compounds **20**, **28** and **38** (Fig. 5 -Figure 6). All three molecules efficiently reduce Compound I directly to Compound II as it is demonstrated in Fig. 5A for the direct conversion of Compound I mediated by compound **38**. The monophasic reaction was very fast and the obtained k_{obs} values were linearly dependent



Scheme 2. Synthesis of piperazine derivatives.



Reagents and conditions: (i) NaBH₃CN, acetic acid, EtOH (ii) BBr₃, DCM

Scheme 3. Synthesis of phenylmethylpiperidine derivatives.

on the electron donor concentration thus allowing the calculation of the apparent bimolecular rate constant (k_2) at pH 7.0 (i.e. $1.4 \times 10^7 \text{ M}^{-1} \text{ s}^{-1}$) (Fig. 5B and C). In comparison to compound **38** the corresponding k_2 values of compounds **20** and **38** were reduced by ~60% and ~90%, respectively (Table 3).

Compound II is also able to oxidize compounds **20**, **28** and **38**, but the corresponding apparent bimolecular rate constants (k_3) are at least three orders of magnitude slower ranging between from $1.4 \times 10^3 \text{ M}^{-1} \text{ s}^{-1}$ to $4.8 \times 10^3 \text{ M}^{-1} \text{ s}^{-1}$ (Fig. 5D–F). As a consequence, these compounds mediate the accumulation of Compound II which is reflected by high k_2/k_3 ratios (Table 3). Kinetics study demonstrated that the entire best active synthesized inhibitors behaved as good one-electron donors for Compound I while their rates of reaction with Compound II shift the reaction to the peroxidase cycle and decreased the production of HOCl.

2.5. Serotonin reuptake inhibition

Because compound **38** carries an indole ring and has a structure related to serotonin, it was tested for inhibition of SERT (together with compounds **20** and **28** for comparison) [73] (Fig. 6) (Table 3). Compound **38** is a weak inhibitor of SERT with a calculated $K_i = 0.8 \text{ } \mu\text{M}$, compared to $11 \text{ } \mu\text{M}$ and $14 \text{ } \mu\text{M}$ for compounds **20** and **28**, respectively. The specificity index K_i/IC_{50} (SERT versus MPO) was then measured. Lower K_i/IC_{50} values demonstrate dual inhibition activity against both SERT and MPO, while higher values prove that the synthesized compounds are selective for MPO, $K_i/IC_{50} = 14.8$ of compound **38** shows selectivity for MPO versus SERT 3.5 times

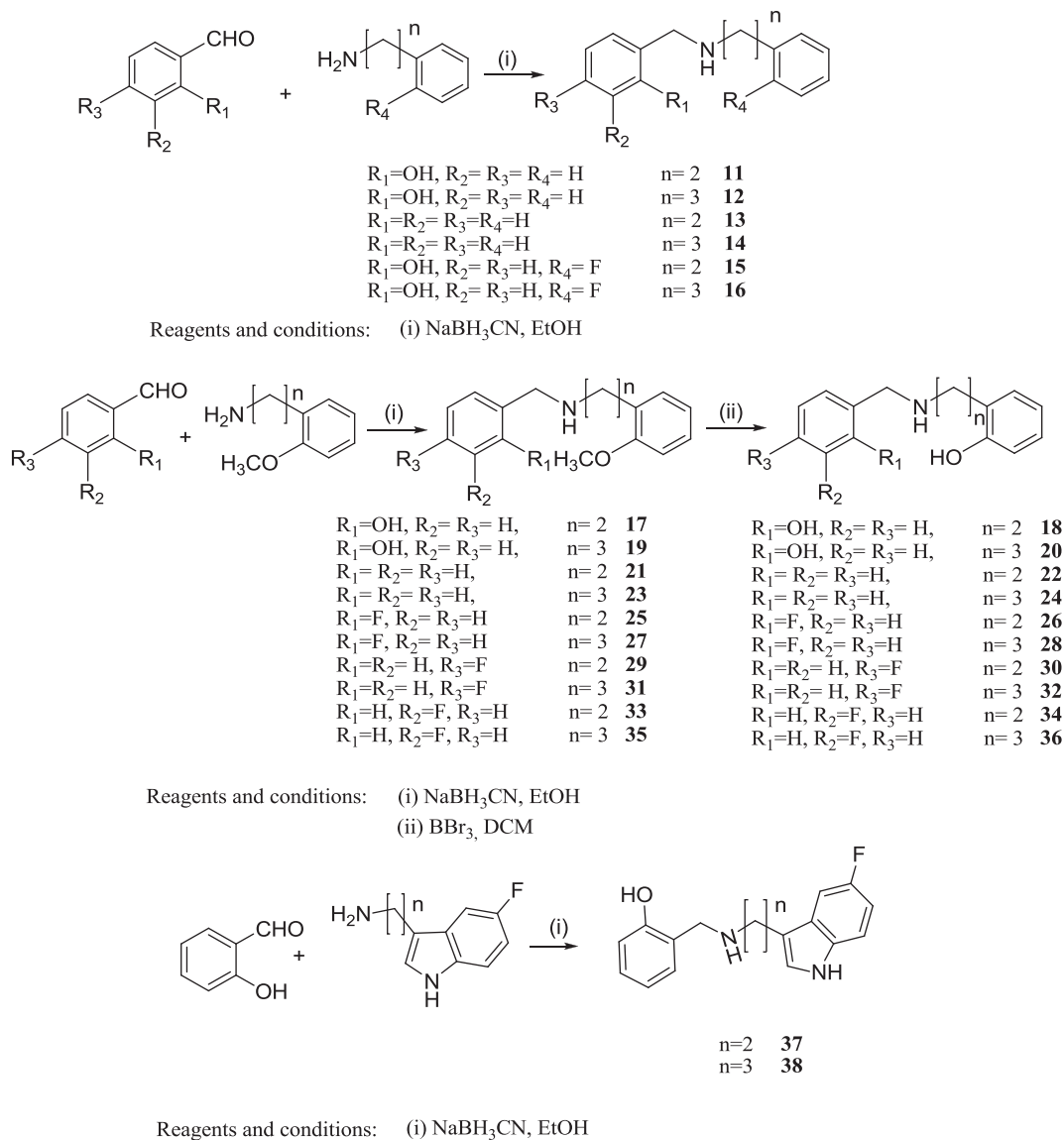
more compared to **S1** a non-selective MPO/SERT inhibitor (for structure of S1 see Fig. 1). Other good inhibitors were more selective on MPO versus SERT than compound **38** but with lower activity (compounds **20** and **28**) (Table 3).

2.6. Electron density maps

Next, we calculated electron density maps and the nucleophilicity of compounds **20**, **28** and **38** in order to predict the site of oxidation (Supplementary materials). Obtained data demonstrated that the oxidation happens preferentially at the benzene ring B (compounds **20** and **28**) or the indole ring (compound **38**). This is also reflected by the fact that the spin density of the oxidized compounds is also located at benzene ring B or the indole cycle (Fig. 7).

2.7. Determination of redox potentials

Finally, we determined the one-electron reduction potential of the putative inhibitors by cyclic voltammetry (reference electrode Ag/AgCl, 3 M NaCl; working electrode glassy carbon) in phosphate buffer, pH 7.4. $E^{o'}$ values were obtained by converting redox potentials from Ag/AgCl, 3 M NaCl to normal hydrogen electrode NHE by adding +198 mV. The corresponding $E^{o'}$ for most of the compounds varied between 807 mV and 1100 mV (Table 1). For compounds, which were unable to inhibit the chlorination activity of MPO (compounds **2**, **3**, **13**, **14**, **21**, **23**, **25**, **27**, **29**, **31**, **33**, **35**) the standard reduction potential could not be determined because the



Scheme 4. Synthesis of Bis-Arylalkylamine and indole derivatives.

E° values were out of the measuring range (>1.2 V). The standard reduction potentials of the relevant redox couples of MPO have been published to be 1.35 V (Compound I/Compound II) and 0.97 V (Compound II/ferric MPO), respectively [72,74–76]. This clearly demonstrates that the one-electron oxidation by Compound I of all inhibiting compounds is favorable, although there is no clear correlation between IC_{50} and E° values.

3. Discussion

Upon virtual screening of large databases [32] bis-2,2'-[(dihydro-1,3(2*H*,4*H*)-pyrimidinediyl)bis(methylene)]phenol (**A1**) was detected to act as potential inhibitor of the chlorination activity of MPO. In this work we used **A1** as a lead compound for pharmacomodulation in order to improve its properties and understand the mechanism of interaction and inhibition. The general structure of the novel series of compounds comprised two aromatic rings A and B (with hydrogen bonding groups on each) which are bridged by at least one amino group either within a heterocyclic structure (ring C) (**A1** and compounds **2–10**) or as part of an open aliphatic bridge

(compounds **11–38**).

Upon substitution of aromatic ring A at positions R_1 , R_2 or R_3 by either hydrogen, fluorine or the hydroxyl group as well as of aromatic ring B at position R_4 with either hydrogen, fluorine, hydroxyl or methoxy groups we aimed at investigating the importance of these functionalities for making non-covalent interactions within the substrate access channel and the heme cavity of MPO. Generally, this work clearly underlined the importance of the presence of hydroxyl groups on both aromatic rings for maintenance of the inhibition capacity. Independent of the nature of bridge between rings A and B (piperidine or piperazine or linear bridge), compounds without any hydroxyl group on the aromatic rings were extremely poor inhibitors (compounds **5–10**) or completely lost the capacity to interfere with MPO activity (compounds **2, 3, 13, 14, 21, 23, 25, 27, 29, 31, 33** and **35**, respectively). This might be related to decreased binding affinity (e.g. loss of interactions formed by hydroxylated rings) and/or an increase in the standard reduction potential of the corresponding compounds. This work clearly demonstrated that the inhibition capacity is related to the ability of the compounds to donate electrons to MPO Compound I. The

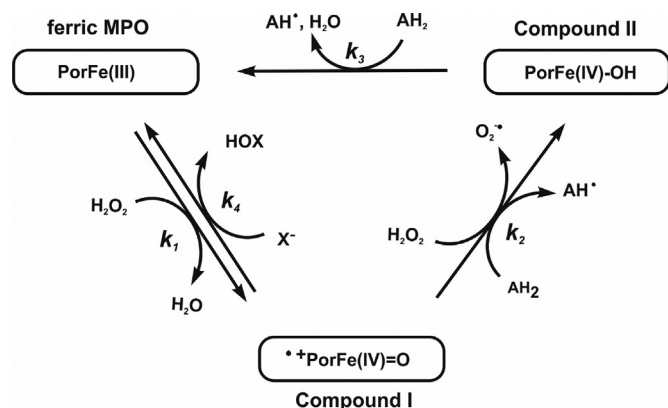


Fig. 4. Peroxidase and halogenation cycle of myeloperoxidase. Upon reaction of the ferric protein with hydrogen peroxide Compound I [^{*}PorFe(IV) = O or oxoiron(IV) porphyrin radical cation] is formed (Reaction 1). In the peroxidase cycle one electron donors (AH₂) reduce Compound I to Compound II (Reaction 2) and Compound II to the ferric enzyme (Reaction 3). The transition of Compound I to Compound II [PorFe(IV) = O or oxoiron(IV)] is also mediated by H₂O₂ as one-electron donor. In the halogenation cycle Compound I is directly reduced by halides (X⁻) thereby releasing hypohalous acids (HOX) (Reaction 4).

aromatic ring B linked to longer bridge has been shown to be the main oxidation site. Having a methoxy group instead of a hydroxyl group on ring B significantly increased the reduction potential of the corresponding compounds thereby losing the inhibition capacity despite the fact that those compounds exhibited the same interaction pattern and still bound to the heme cavity. Generally, the impact of substitution of ring B on MPO inhibition is more pronounced than that of ring A. Upon removing of aromatic ring B (compounds **9** and **10**) the inhibition capacity was almost lost.

Furthermore, our study revealed that (i) the presence of one amino group on the bridge (independent of being part of a cyclic structure or an aliphatic chain) between rings A and B is sufficient for the establishment of binding to Glu102 and (ii) that the presence of three methylene groups between the secondary amine and the aromatic ring B improved the inhibition of chlorination and thus decreased the IC₅₀ values. These results show that the hydroxyl group on ring B is more important than on ring A. Indeed, the hydroxyl group in aromatic ring B in compound **24** increases the activity by nearly four times compared to compound **12** which has hydroxyl group on aromatic ring A. This indicates that the distance between the hydrogen bonding group of ring B and the amino group is very important. Additionally, the docking poses of active compounds **26**, **28**, **30**, **32**, **34** and **36**, show ionic and hydrogen bonding interactions between Glu102 and hydroxyl group on ring B while the smaller volume of fluorine on ring A allows the stacking pose of ring A.

This is also observed in our new compounds **37** and **38** which carry a fluorindole ring instead of the aromatic ring B obtained by hybridization of hit **A1** and the potent MPO inhibitors fluoro-tryptamine derivatives [45]. Compound **38** is the best inhibitor of this study, its IC₅₀ is 54 nM, which is 10-times lower compared to the lead compound **A1**, despite showing similar interactions with Glu102 and Arg239 as well as similar score values and similar stacking compared to both **HX1** and **A1**. Moreover, upon elimination of this hydroxyl group in compound **38** (Table 3, compound **S1**) the inhibition capacity is improved (IC₅₀ = 13 nM) [45]. This could be related with the architecture and composition of the substrate access channel of MPO which at its entrance to the heme cavity forms a funnel shaped hydrophobic pocket. Thus elimination of the hydroxyl group or exchange by fluorine increases the hydrophobicity and improve the inhibition activity towards MPO. However,

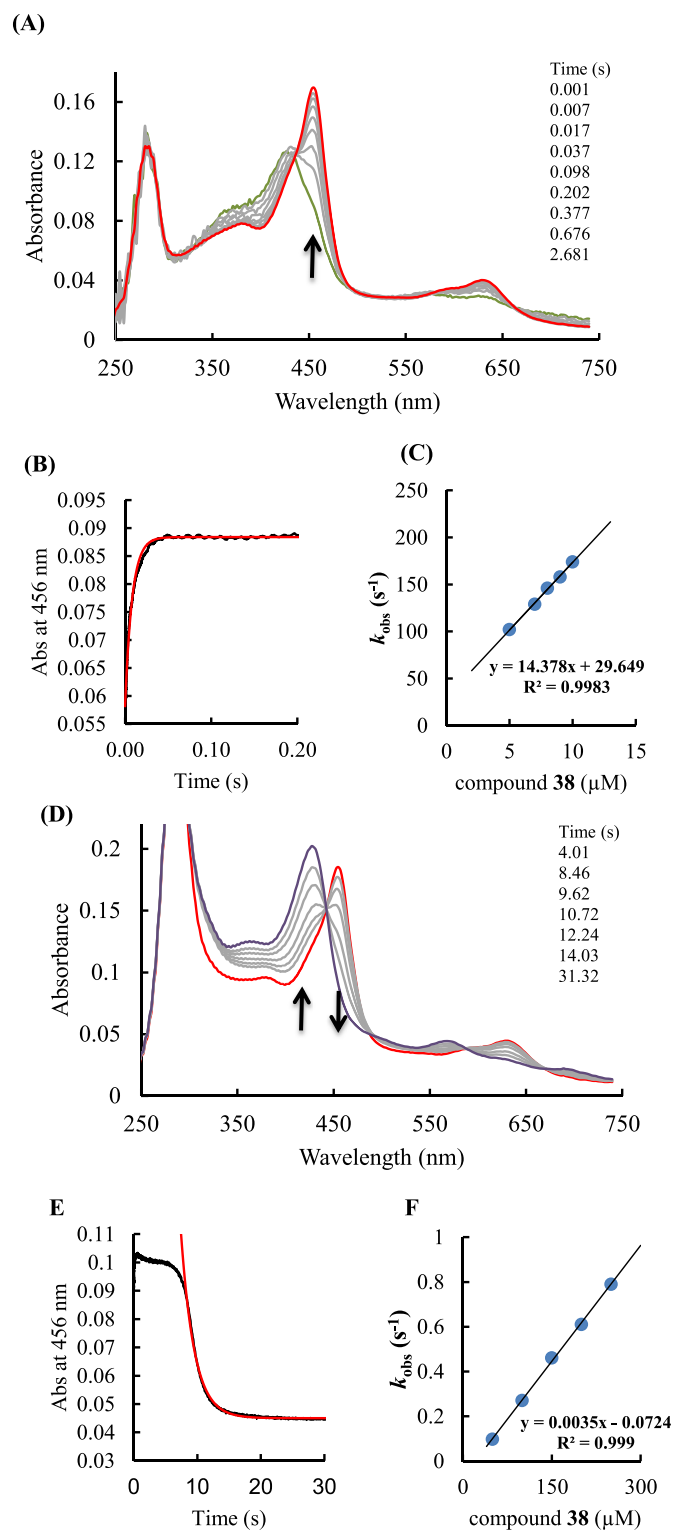


Fig. 5. Reaction of MPO Compounds I and II with compound 38. (A) Spectral changes upon mixing 1.0 μM MPO Compound I with 2 μM compound **38** at pH 7.4 and 25 °C. (B) Typical time trace and single-exponential fit (red) at 456 nm for the reaction between 1 μM Compound I and 8 μM compound **38**. (C) Pseudo-first-order rate constants for Compound I reduction plotted against concentration of compound **38**. (D) Spectral changes of reduction of 2 μM Compound II by 250 μM compound **38** at pH 7.4 and 25 °C. (E) Typical time trace and single-exponential fit (red) of the reaction between 1 μM MPO Compound II and 250 μM compound **38** followed at 456 nm. (F) Pseudo-first-order rate constants for the reduction of MPO Compound II plotted against concentration of compound **38**. (For interpretation of the references to colour in this figure legend, the reader is referred to the web version of this article.)

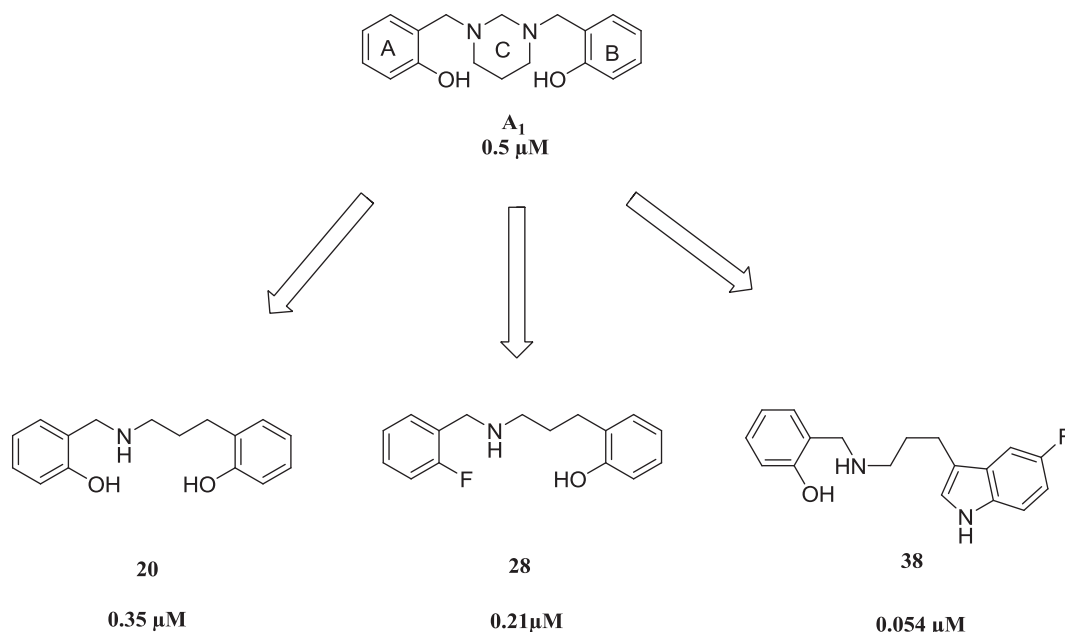


Fig. 6. Structures of the most potent synthesized MPO inhibitors derived from compound A1.

Table 3
 Apparent bimolecular rate constants of MPO Compound I (k_2) and Compound II reduction (k_3) by compounds **20**, **28** and **38**. Additionally, values of 5-HT reuptake inhibition and MPO inhibition (IC_{50} in μM) are included. ND = no data available.

Compound	Compound I reduction ($\text{M}^{-1}\text{s}^{-1}$)	Compound II reduction ($\text{M}^{-1}\text{s}^{-1}$)	Ratio of k_2/k_3	MPO IC_{50} (μM)	SERT K_i (μM)	SERT $K_i/\text{MPO IC}_{50}$
20	1.5×10^6	4.8×10^3	313	0.35 ± 0.05	11 ± 2	31.4
28	5.7×10^6	1.4×10^3	4071	0.27 ± 0.03	14 ± 3	51.8
38	1.4×10^7	3.5×10^3	4000	0.054 ± 0.007	0.8 ± 0.2	14.8
S1^a	ND	ND	ND	0.013 ± 0.002	0.05 ± 0.02	4.1

^a **S1** has the same structure as compound **38** but lacks the hydroxyl group.

the introduction of the hydroxyl group is accompanied by a dramatic decrease of the SERT inhibition leading to an increase of the selectivity of this compound as the selectivity increase from 4 (compound **S1**) to 14 (compound **38**) (Table 3). It is also noteworthy that the low IC_{50} at submicromolar range obtained in this study is compatible with an enzyme inhibition and not a simple scavenging effect towards hypochlorous acid. Indeed, the amount of MPO, chloride and hydrogen peroxide in the MPO inhibition assay allow us to produce around $60 \mu\text{M}$ of hypochlorous acid while the inhibitors act at concentration 1000 fold less.

The present study also supports the difficulty to predict the inhibitory effect on MPO using the scoring functions, regardless of the receptor structure used, which can reasonably not discriminate between the different ligands. One of the possible reasons is that factors other than binding contribute in the MPO inhibition. Docking calculations provide valuable information about binding poses and non-covalent interactions but in case of this oxidoreductase also the redox chemistry of both the enzyme and the ligands are very important for inhibition. Our mechanistic study clearly underlines that the inhibiting compounds act as one-electron donors for Compound I and Compound II of MPO. This was demonstrated for the best inhibitors, i.e. compounds **20**, **28** and **38**. Compound I of MPO is known to be one of the strongest enzymatic oxidants with a standard reduction potential of 1.35 V for the redox couple Compound I/Compound II. This compares with 0.97 V for the couple Compound II/ferric MPO, respectively [72,75–77]. The results show that all of the active compounds have

E° values less than 1.2 V which allows an oxidation of the molecule by Compound I. As a consequence, the determined apparent bimolecular rate constants for Compound I reduction (k_3) of compounds **20**, **28** and **38** are shown to be about 3 magnitudes of order higher compared to those for Compound II reduction (k_4). The resulting high ratios of k_3/k_4 lead to accumulation of Compound II which is the inactive form of MPO shifting the MPO from the chlorination cycle to the peroxidase cycle (Fig. 4). Subsequently, our inhibitors are reversible MPO inhibitors [32,35,78] and substrates for MPO and must be quickly oxidized by Compound I of MPO to accumulate Compound II. As mentioned above substitution of hydroxyl groups by methoxy groups and fluorine renders the corresponding molecules to weak electron donors and thus poor MPO inhibitors. All inactive compounds had reduction potentials >1.2 V.

Thus, the key structural elements of these good reversible MPO inhibitors include: 1) Two aromatic rings with at least one hydroxyl group, which is important for building hydrogen bonds with surrounding residues. In this context, ring A and ring B are essential to keep the activity but the hydroxyl group on ring A is less crucial than the hydroxyl group on ring B since aromatic ring B linked to longer bridge chain (3 carbons) allows oxidation site of those molecules. 2) One amino group on the bridge between the two rings for interaction with Glu102 that is crucial for optimum ligand binding [3], and 3) An overall reduction potential ($0.85 \text{ V} < E^\circ < 1.2 \text{ V}$) that allows rapid conversion of Compound I to Compound II in order to outcompete the two-electron reduction of Compound I by chloride [3].

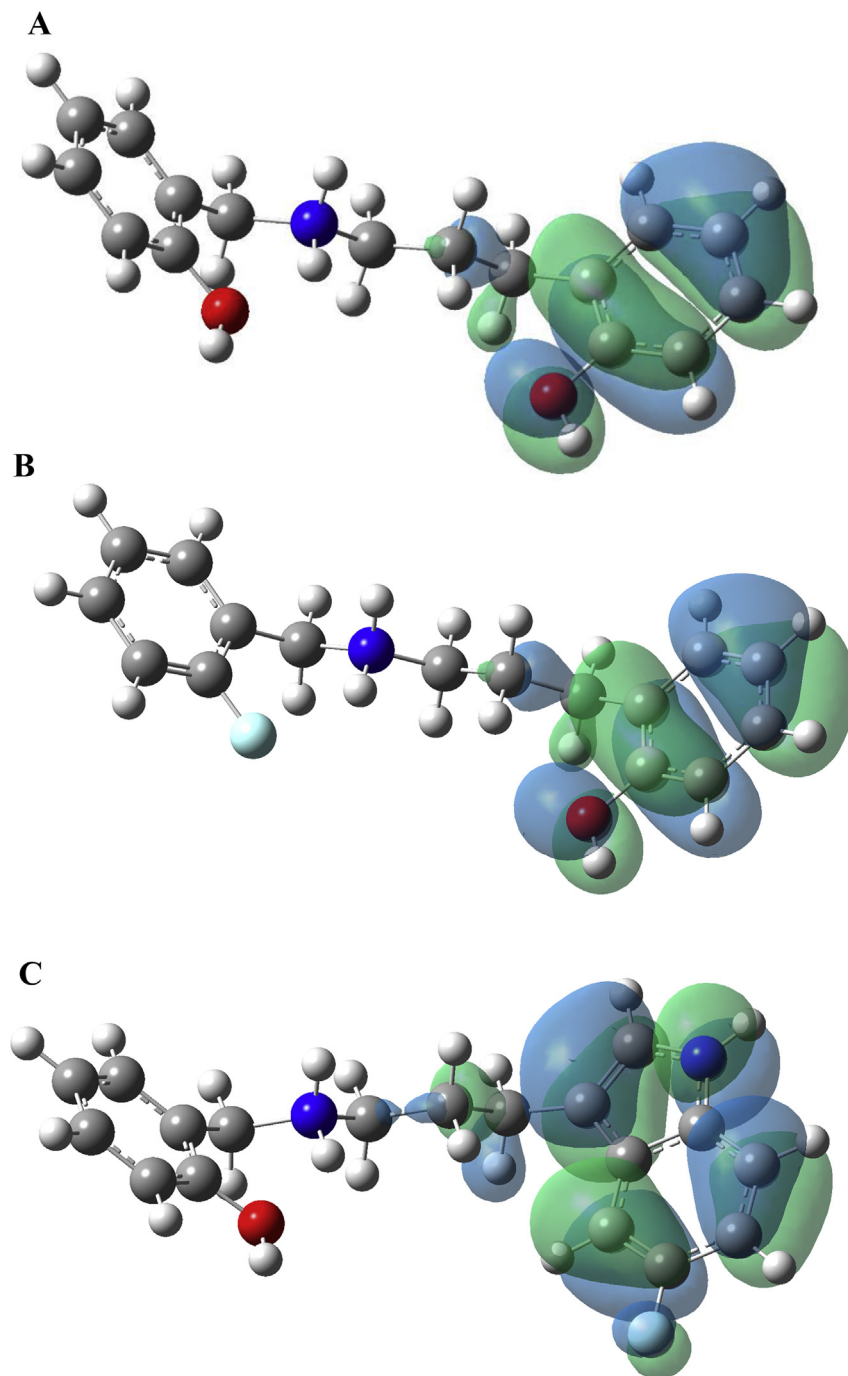


Fig. 7. Electron density calculations: HOMO of the ligands shows that the oxidation probably happens at the green spots of ring B or indole cycle. (A) Compound **20**, (B) Compound **28** (C) Compound **38**. (For interpretation of the references to colour in this figure legend, the reader is referred to the web version of this article.)

4. Conclusion

To sum up, new chemical entities for MPO inhibition were found. Structure-based drug design has been successful to create better inhibitors. They act as electron donors of the oxidoreductase and efficiently shift MPO from the chlorination cycle to the peroxidase cycle (Fig. 4) and thus act as reversible MPO inhibitors [32,35,78]. Eight compounds were more active than the starting hit **A1** with submicromolar activities. The best compound **38** is 10 times more active than the starting hit with higher selectivity

toward MPO versus SERT compared to **S1**. Other compounds namely compound **28** proved to be the most selective one toward peroxidase (13 times more than compound **S1**) and 2 times more active than the hit **A1**. Above all, the pharmacomodulation has given new bis-arylpropylamine derivatives which were first introduced as novel MPO inhibitors. These bis-arylpropylamine derivatives are promising novel MPO inhibitors and it will be interesting to probe their efficacy in *in vivo* model systems in the future.

5. Experimental section: materials and methods

5.1. Synthesis

^1H and ^{13}C NMR spectra were taken on a Bruker Avance 300 M Hz spectrometer (Wissemburg, France) at 293 K. Chemical shifts (δ) are given in parts per million (ppm) relative to tetramethylsilane (TMS), and the coupling constants are expressed in hertz. Infrared spectroscopic analysis was performed with a Shimadzu (Kyoto, Japan) IRAffinity-1 spectrophotometer equipped with ATR system and the peak data are given in cm^{-1} . Mass spectrometric data were obtained on a QTOF 6520 (Agilent, Palo Alto, CA), positive mode, electrospray ionization (ESI), mode time of flight (TOF), by diffusion of 0.5 mL/min, by mobile phase 0.1 M $\text{HCOOH}/\text{CH}_3\text{OH}$ (50:50) (VCAP 3500 V, source T, 350 °C; fragmentation, 110 V; skimmer, 65 V). All reactions were followed by thin-layer chromatography (TLC) carried out on Fluka (Bornem, Belgium) PET foils silica gel 60, and compounds were visualized by UV and by spraying Van Urk reagent (0.125 g of *p*-dimethylaminobenzaldehyde dissolved in 100 mL of 65% sulfuric acid with addition of 0.1 mL of 5% ferric chloride). Flash chromatography was performed with silica (63–200 μm) from MP Biomedicals (Santa Ana, CA) or with neutral alumina (Al_2O_3 , 50–200 μm) purchased from Merck. Organic solutions were dried over Na_2SO_4 and concentrated with a Buchi rotatory evaporator (Flawil, Switzerland). Starting materials: 3-(2-methoxybenzyl)-piperidine was purchased from (Bio Block; USA), 3-(2-fluorophenyl)-propylamine, 3-(2-ethylamine)-5-fluoro-1*H*-Indole, 3-(3-propylamine)-5-fluoro-1*H*-Indole were purchased from Enamine Building Blocks (Monmouth, Jct, USA), 3-(2-methoxyphenyl)-propylamine was purchased from ChemBridge Building Block Library (San Diego, CA, USA), piperazine was purchased from TCI (Japan), 2-(2-methoxyphenyl)-ethylamine, 2-(2-fluorophenyl)-ethylamine, 3-phenylpropylamine, 2-phenylethylamine were purchased from (Sigma Aldrich, Bornem, Belgium). Purity was determined with liquid chromatography (LC) with diode-array detection (DAD) (Waters, Milford, MA, USA) on a 150 mm \times 4.6 mm Symmetry C₈ column at a mobile phase flow rate of 1 mL/min. The mobile phase was a mixture of methanol (700 mL) and a KH_2PO_4 solution (0.07 M in methanol 5%, 300 mL) adjusted to pH 3.0 with a 34 wt % H_3PO_4 solution. The purity was $\geq 95\%$ for all compounds.

5.1.1. Chemical synthesis procedures

5.1.1.1. Synthesis procedure of compound 1. To a solution of benzaldehyde (5 mmol, 0.51 g) in 50 ml of ethanol an ethanolic solution of 1,3-diaminopropane (2.5 mmol, 0.19 g) was added dropwise during 10 min at room temperature. After 2 h sodium cyanoborohydride (10 mmol, 0.63 g) was added and left overnight. The solution was evaporated and the residue was taken up with 10 ml of water and extracted two times with 25 ml of CH_2Cl_2 . The organic layer was dried over anhydrous Na_2SO_4 , filtered and evaporated. The crude material was purified by flash chromatography on silica gel by using a mixture of $\text{CH}_2\text{Cl}_2/\text{MeOH}$ (95:5) to afford colorless oil (0.61 g, yield 96%).

5.1.1.2. Synthesis procedure of compound 2. To compound 1 (0.61, 2.25 mmol) dissolved in ethanol (50 ml) a solution of formaldehyde 37 wt % in H_2O (0.23 ml, 4.5 mmol) was added dropwise at room temperature and the reaction left overnight. The crude mixture was evaporated, CH_2Cl_2 was added (25 ml) and the organic layer was washed with water, dried over anhydrous Na_2SO_4 , filtered and evaporated. The crude material was purified by flash chromatography on silica gel SiO_2 by using a mixture of $\text{CH}_2\text{Cl}_2/\text{MeOH}$ (99:1) to afford white pale solid (0.46 g, yield 73%).

5.1.1.3. Synthesis procedure of compound 3. To a solution of *N,N'*-trimethyleneurea (0.50 g, 5 mmol) in 1,4-dioxane (5 ml) was added to NaH 95% (0.24 g, 10 mmol) and benzyl chloride (1.27 g, 10 mmol) dissolved in 45 ml of 1,4-dioxane at 0 °C. The reaction mixture was refluxed overnight and cooled to room temperature. The solvent was evaporated under reduced pressure. CH_2Cl_2 was added, the organic layer was washed with water, dried over anhydrous Na_2SO_4 , filtered and evaporated. The crude material was purified by flash chromatography on silica gel SiO_2 by using a mixture of $\text{CH}_2\text{Cl}_2/\text{MeOH}$ (95:5) to afford white solid (1.07g, yield 76%).

5.1.1.4. General procedure of synthesis for compounds 4–7. A solution of anhydrous piperazine (0.86 g, 10 mmol) in EtOH (10 ml) was added dropwise to solution of acetic acid (10 mmol) and the suitable aldehyde (20 mmol) in EtOH (40 ml), then sodium cyanoborohydride NaBH_3CN (1.26 g, 20 mmol) was added after 1 h, and the resulting solution was stirred overnight. The solution was evaporated and the residue was taken up with 20 ml of water and extracted two times with 25 ml of CH_2Cl_2 , the organic layer was washed with water, dried over anhydrous Na_2SO_4 , filtered and evaporated. The crude material was purified by flash chromatography using $\text{CH}_2\text{Cl}_2/\text{MeOH}$ to afford the desired compound (see [Supplementary materials](#)).

5.1.1.5. Synthesis procedure of compound 8. A solution of piperazine (0.86 g, 10 mmol) in CH_2Cl_2 (10 ml) was added dropwise to solution of triethylamine (2.22 g, 22 mmol) and benzylchloride (2.53 g, 20 mmol) in 40 ml of CH_2Cl_2 , and the resulting suspension was stirred overnight. The mixture was evaporated under reduced pressure, the residue extracted by ethyl acetate EtOAc (50 ml), the organic layer was washed with water, dried over anhydrous Na_2SO_4 , filtered and evaporated. The crude material was purified by flash chromatography (silica gel SiO_2) using EtOAc/MeOH (80:20). The silicagel was taken up from the column, mixed with a mixture of EtOAc/MeOH (60:40), filtered and the resulted solvent was evaporated to afford white solid (0.47 g, yield 18%).

5.1.1.6. Synthesis procedure of compound 9. A solution of piperidine (0.85 g, 10 mmol) and glacial acetic acid (0.60 g, 10 mmol) in EtOH (40 ml) was added dropwise to a solution of salicylaldehyde (1.22 g, 10 mmol) in EtOH (10 ml). After 20 min NaBH_3CN (1.26 g, 20 mmol) was added and the reaction was left overnight. The reaction mixture was acidified by a solution of HCl 1 N to arrive to pH = 2. The solvent was evaporated under reduced pressure, and 40 ml of water was added and then a solution of KOH 4 N was added until pH = 7. The water solution was extracted with Et_2O twice (30 ml) and the organic solvent was washed by brine twice (20 ml), dried over anhydrous Na_2SO_4 , filtered and evaporated. The crude material was purified by flash chromatography on silica gel SiO_2 (gradient 90:10 to 80:20 EtOAc: NH_3 in MeOH 10%) to afford white pale solid (0.97 g, yield 51%).

5.1.1.7. Synthesis procedure of compound 10. A solution of boron tribromide in CH_2Cl_2 (1.03 g, 4.07 mmol) was added dropwise to a solution of 3-(2-methoxybenzyl)-piperidine (0.31 g, 1.5 mmol) in CH_2Cl_2 (50 ml) at -78 °C. Then the temperature of the mixture let to come back to RT over a period of 1h and the reaction was stirred overnight. An aqueous saturated solution of NaHCO_3 was added dropwise at 0 °C and then pH was adjusted to reach the range of 7–8 with the same solution, the organic layer was separated and the water layer was extracted by CH_2Cl_2 (3 \times 40 ml). The combined organic layers were dried using (Na_2SO_4) and evaporated under reduced pressure. Purification for the crude material was done by flash chromatography on Al_2O_3 by using $\text{CH}_2\text{Cl}_2/\text{NH}_3$ solution in MeOH 1%/(95:5) to afford white solid (0.06 g, yield 20%).

5.1.1.8. General procedure of synthesis for compounds (11–16) (17,19, 21,23,25,27,29,31,33,35,37,38). A solution of an arylalkylamine or an indole derivative (10 mmol) in EtOH (5 ml) was added dropwise to a solution of aldehyde (10 mmol) in 50 ml of EtOH, after one hour NaBH₃CN was added (20 mmol) the resulting solution was stirred overnight. The solution was evaporated and the residue was taken up with water and extracted with CH₂Cl₂. The organic layer was dried over anhydrous Na₂SO₄, filtered and evaporated. The crude material was purified by flash chromatography by using silica gel SiO₂ (for defined eluent percentage see [Supplementary materials](#)) to afford desired compound.

5.1.1.9. General procedure of synthesis for compounds (18, 20, 22, 24, 26, 28, 30, 32, 34, 36). A solution of boron tribromide in CH₂Cl₂ (4.4 mmol) was added dropwise to a solution of compound resulting from the previous general procedure (bis-arylalkylamine derivative) (1.5 mmol) in CH₂Cl₂ (50 ml) at –78 °C and the temperature of the mixture was left to arrive RT over a period of 1 h and the reaction was stirred overnight. An aqueous saturated solution of NaHCO₃ was added dropwise at 0 °C and then pH was adjusted to reach a range of 7–8 with the same solution, then the reaction mixture was extracted by CH₂Cl₂; the combined organic layers were separated, dried over (Na₂SO₄), and evaporated under reduced pressure. Purification for the crude material was done by flash chromatography of silica gel (see [Supplementary materials](#)) to afford desired compound.

5.2. Docking experiments

The X-ray structure of human MPO complexed to cyanide and thiocyanate (PDB code 1DNW) and the human MPO complexed to **HX1** (PDB code 4C1M) were used as the receptors targets in docking studies [52,56]. The X-ray water and other ligand molecules were removed from the active site. The ligand input files were prepared according to the following procedure. The initial 3D structures of the ligands were generated with the Ligprep module from Schrodinger [79] [32] and the ligand partial charges were ascribed by use of the OPLS force field [80]. The Epik program was used to predict different protonation states of all ligands [81]. Docking was performed with the program (version 6.1), which approximates a systematic search of positions, orientations, and conformations of the ligand in the receptor binding site by use of a series of hierarchical filters (www.schrodinger.com). The Glide XP docking protocol and scoring function were used. The remaining parameters were set to their default values.

5.3. Taurine chlorination assay

The assay is based on the production of taurine chloramine produced by the MPO/H₂O₂/Cl[–] system in the presence of a selected inhibitor at different concentrations as described by Van Antwerpen et al., 2007 [82]. The reaction mixture contained the following reagents in a final volume of 200 µL: 10 mM phosphate buffer (pH 7.4, 300 mM NaCl), 15 mM taurine, compound to be tested (up to 20 µM), and a fixed amount of recombinant MPO (6.6 µL of MPO batch solution diluted 2.5 times, 40 nM). When necessary, the volume was adjusted with water. This mixture was incubated at 37 °C and the reaction was initiated with 10.0 µL of H₂O₂ (100 µM). After 5 min, the reaction was stopped by the addition of 10 µL of catalase (8 units/µL). To determine the amount of taurine chloramine produced, 50 µL of 1.35 mM solution of thionitrobenzoic acid was added and the volume was adjusted to 300 µL with water. Then the absorbance of the solutions was measured at 412 nm with a microplate reader, and the curve of absorbance as a function of inhibitor concentration was plotted.

IC₅₀ values were then determined by standard procedures, taking into account the absence of hydrogen peroxide as 100% inhibition and the absence of inhibitors as 0% inhibition.

5.4. Transient-state kinetics

Highly purified MPO with purity index (A_{430}/A_{280}) of at least 0.86 was purchased from Planta Natural Products (<http://www.planta.at/>). Its concentration was calculated by use of $\epsilon_{430} = 91 \text{ mM}^{-1} \text{ cm}^{-1}$. Enzyme concentration was determined by using the extinction coefficient $112,000 \text{ M}^{-1} \text{ cm}^{-1}$ at 412 nm [83]. Hydrogen peroxide obtained from a 30% solution was diluted and the concentration was determined by absorbance measurement at 240 nm, where the extinction coefficient is $39.4 \text{ M}^{-1} \text{ cm}^{-1}$. Inhibitor stock solutions were prepared in dimethyl sulfoxide and stored in dark flasks. Dilution was performed with 200 mM phosphate buffer, pH 7.4, to a final DMSO concentration of 2% (v/v) in all assays [84].

The multimixing stopped-flow measurements were performed with the Applied Photophysics (UK) instrument SX-18MV. When 100 µL was shot into a flow cell having a 1 cm light path, the fastest time for mixing two solutions and recording the first data point was 1.3 ms. Kinetics were followed both at single wavelength and by use of a diode-array detector. At least three determinations (2000 data points) of pseudo-first-order rate constants (k_{obs}) were performed for each substrate concentration (pH 7.4, 25 °C) and the mean value was used in the calculation of the apparent second-order rate constants, which were calculated from the slope of the line defined by a plot of k_{obs} versus substrate concentration. To allow calculation of pseudo-first-order rates, the concentrations of substrates were at least 5 times in excess of the enzyme.

Conditions of MPO Compound I formation were described recently [85]. Typically, 8 µM MPO was premixed with 80 µM H₂O₂, and after a delay time of 20 ms, Compound I was allowed to react with varying concentrations of alkylindole derivative in 200 mM phosphate buffer, pH 7.4. The reactions were followed at the Soret maximum of Compound II (456 nm). Compound II formation and reduction could be followed in one measurement. The resulting biphasic curves at 456 nm showed the initial formation of Compound II (increase in absorbance at 456 nm) and its subsequent reduction to native MPO by the alkylindole derivatives (decrease in absorbance at 456 nm).

5.5. Assessment of 5HT reuptake inhibition

Inhibition assessment of 5-HT reuptake was performed as follows: The mammalian expression plasmid pcDNA3.1 containing human 5-HT transporter (hSERT) cDNA has been described previously by Kristensen et al. [86]. HEK-293 MSR cells (Invitrogen) were cultured as monolayers in Dulbecco's modified Eagle's medium (BioWhittaker) supplemented with 10% fetal calf serum (Invitrogen), 100 units/mL penicillin, 100 µg/mL streptomycin (BioWhittaker), and 6 µg/mL Geneticin (Invitrogen) at 95% humidity, 5% p(CO₂), and 37 °C. Cells were detached from the culture flasks by Versene (Invitrogen) and trypsin/EDTA (BioWhittaker) treatment for subculturing or seeding into white TC-microtiter plates (Nunc). Transfection and measurement of [³H]5-HT (PerkinElmer Life Sciences) uptake was performed as described by Larsen et al. [87], except that HEK-293 MSR cells (Invitrogen) were used instead of COS-1 cells.

5.6. Determination of redox potentials

The experiments were achieved in a conventional three-electrode cell at $25 \pm 2 \text{ }^\circ\text{C}$, associated with a potentostat

Epsilon (BASi, West Lafayette, IN). The working electrode was a glassy carbon disk polished with 0.05 mm alumina (Metkron) before each run, for linear cyclic voltammetry measurements. The auxiliary electrode was a platinum wire. The reference electrode was Ag/AgCl (3 M NaCl). The inhibitors were dissolved in 0.1 M phosphate buffer, pH 7.4. The solutions were diluted by the same buffer until inhibitor concentration of 1×10^{-4} M. Cyclic voltammograms were obtained by a single cycle performed at a scan rate of 100 mV s^{-1} . For the scan rate studies, the scan rate was varied from -200 to 1000 mV s^{-1} . $E^{\circ'}$ values were obtained by converting redox potentials from Ag/AgCl, 3 M NaCl to normal hydrogen electrode (NHE) by adding $+198 \text{ mV}$. Because the oxidation of our compounds was irreversible, it is difficult to determine their $E^{\circ'}$ values. However, in our case $E^{\circ'}$ values are slightly less than E' [45].

5.7. Electron density maps

Calculations of electron density maps of three best selected active compounds (**20**, **28**, **38**) have been conducted in order to predict their oxidation sites, the non-condensed Fukui function [88] $f^-(r)$, calculated [89] as the difference between the electron densities of the ligand having N_0 and N_0-1 electrons ($f^-(r) = \rho(r)(N_0) - \rho(r)(N_0 - 1)$), indicates the site in a molecule having the maximum nucleophilic power, and thus it indicates the place from where the electron will preferentially be donated during oxidation. $f^-(r)$ is related to the highest occupied orbital (HOMO) electron density of the molecule. In accordance with the location of the HOMO orbital, the density difference plots giving $f^-(r)$ obtained on selected compounds shows where the oxidation happens preferentially (see [Supplementary materials](#)). The spin density, obtained as the difference between the electron density of the alpha and beta electrons were calculated on the radical form of the compounds.

The geometries of selected (**20**, **28**, **38**) synthesized compounds are optimized at the B3LYP/6-311G(d,p) level. Frequency calculations were performed to ensure a local minimum. The electron densities and molecular orbitals are calculated at the B3LYP/6-311G(d,p) level on the optimized geometries. All calculations are performed with Gaussian09 [90].

Author contributions

The manuscript was written in a collaborative mode by all authors. All authors have given approval to the final version of the manuscript.

Acknowledgment

We thank the “Wallonie Bruxelles International” Agency (www.wbi.be) (grant no.: SOR/2011/33449), Fonds David & Alice Van Buuren and the FRS-FNRS for their support. Martine Prévost is a “Maître de Recherche” at the FNRS (Belgian Scientific Research Fund). Cédric Delporte and Jalal Soubhye are research fellows at the FNRS. Additionally, the work was supported by the Austrian Science Foundation (project P25538). Finally, we thank prof. Jean-Michel Kauffmann for his support in the redox potential measurement.

Appendix A. Supplementary data

Supplementary data related to this article can be found at <http://dx.doi.org/10.1016/j.ejmech.2016.07.053>.

References

[1] M. Zamocky, C. Jakopitsch, P.G. Furtmuller, C. Dunand, C. Obinger, The

- peroxidase-cyclooxygenase superfamily: reconstructed evolution of critical enzymes of the innate immune system, *Proteins* 72 (2008) 589–605.
- [2] S.J. Klebanoff, Myeloperoxidase-halide-hydrogen peroxide antibacterial system, *J. Bacteriol.* 95 (1968) 2131–2138.
- [3] P. Van Antwerpen, K. Zouaoui Boudjeltia, Rational drug design applied to myeloperoxidase inhibition, *Free Radic. Res.* 49 (2015) 711–720.
- [4] P.G. Furtmuller, M. Zederbauer, W. Jantschko, J. Helm, M. Bogner, C. Jakopitsch, C. Obinger, Active site structure and catalytic mechanisms of human peroxidases, *Arch. Biochem. Biophys.* 445 (2006) 199–213.
- [5] B.S. van der Veen, M.P.J. de Winther, P. Heeringa, Myeloperoxidase: molecular mechanisms of action and their relevance to human health and disease, *Antioxidants Redox Signal.* 11 (2009) 2899–2937.
- [6] M.J. Davies, Myeloperoxidase-derived oxidation: mechanisms of biological damage and its prevention, *J. Clin. Biochem. Nutr.* 48 (2011) 8–19.
- [7] G. Battistuzzi, J. Stamper, M. Bellei, J. Vlasits, M. Souidi, P.G. Furtmuller, C. Obinger, Influence of the covalent heme-protein bonds on the redox thermodynamics of human myeloperoxidase, *Biochemistry* 50 (2011) 7987–7994.
- [8] M. Zederbauer, P.G. Furtmuller, B. Ganster, N. Moguilevsky, C. Obinger, The vinyl-sulfonium bond in human myeloperoxidase: impact on compound I formation and reduction by halides and thiocyanate, *Biochem. Biophys. Res. Commun.* 356 (2007) 450–456.
- [9] M. Zederbauer, P.G. Furtmuller, S. Brogioni, C. Jakopitsch, G. Smulevich, C. Obinger, Heme to protein linkages in mammalian peroxidases: impact on spectroscopic, redox and catalytic properties, *Nat. Product. Rep.* 24 (2007) 571–584.
- [10] O. Iankovskii, T.E. Dovnar, A.A. Tkachenko, Mechanism of the antimicrobial action of myeloperoxidase, *Role Adsorpt. enzyme target Cell Surf.* (1981) 58–61. *Zhurnal mikrobiologii, epidemiologii, i immunobiologii.*
- [11] J.P. Gaut, G.C. Yeh, H.D. Tran, J. Byun, J.P. Henderson, G.M. Richter, M.L. Brennan, A.J. Lusis, A. Belaouaj, R.S. Hotchkiss, J.W. Heinecke, Neutrophils employ the myeloperoxidase system to generate antimicrobial brominating and chlorinating oxidants during sepsis, *Proc. Natl. Acad. Sci. U. S. A.* 98 (2001) 11961–11966.
- [12] E.L. Thomas, Myeloperoxidase, hydrogen peroxide, chloride antimicrobial system: nitrogen-chlorine derivatives of bacterial components in bactericidal action against *Escherichia coli*, *Infect. Immun.* 23 (1979) 522–531.
- [13] J.E. Smolen, R.J. Hessler, W.M. Nauseef, M. Goedken, Y. Joe, Identification and cloning of the SNARE proteins VAMP-2 and syntaxin-4 from HL-60 cells and human neutrophils, *Inflammation* 25 (2001) 255–265.
- [14] A.J. Kettle, C.C. Winterbourn, Chapter 12 Myeloperoxidase: Structure and Function of the Green Heme Peroxidase of Neutrophils, *Heme Peroxidases*, The Royal Society of Chemistry, 2016, pp. 272–308.
- [15] V. Brinkmann, A. Zychlinsky, Neutrophil extracellular traps: the second function of chromatin? *J. Cell Biol.* 198 (2012) 773–783.
- [16] S.J. Klebanoff, Myeloperoxidase: friend and foe, *J. Leukoc. Biol.* 77 (2005) 598–625.
- [17] R.A. Matthijssen, D. Huugen, N.T. Hoebbers, B. de Vries, C.J. Peutz-Kootstra, Y. Aratani, M.R. Daha, J.W. Tervaert, W.A. Buurman, P. Heeringa, Myeloperoxidase is critically involved in the induction of organ damage after renal ischemia reperfusion, *Am. J. Pathol.* 171 (2007) 1743–1752.
- [18] M.B. Hampton, A.J. Kettle, C.C. Winterbourn, Inside the neutrophil phagosome: oxidants, myeloperoxidase, and bacterial killing, *Blood* 92 (1998) 3007–3017.
- [19] D.K. Choi, S. Pennathur, C. Perier, K. Tieu, P. Teismann, D.C. Wu, V. Jackson-Lewis, M. Vila, J.P. Vonsattel, J.W. Heinecke, S. Przedborski, Ablation of the inflammatory enzyme myeloperoxidase mitigates features of Parkinson's disease in mice, *J. Neurosci. Off. J. Soc. Neurosci.* 25 (2005) 6594–6600.
- [20] R.A. Maki, V.A. Tyurin, R.C. Lyon, R.L. Hamilton, S.T. DeKosky, V.E. Kagan, W.F. Reynolds, Aberrant expression of myeloperoxidase in astrocytes promotes phospholipid oxidation and memory deficits in a mouse model of Alzheimer disease, *J. Biol. Chem.* 284 (2009) 3158–3169.
- [21] W.F. Reynolds, M. Hiltunen, M. Pirskanen, A. Mannermaa, S. Helisalmi, M. Lehtovirta, I. Alafuzoff, H. Soininen, MPO and APOEepsilon4 polymorphisms interact to increase risk for AD in Finnish males, *Neurology* 55 (2000) 1284–1290.
- [22] W.F. Reynolds, J. Rhee, D. Maciejewski, T. Paladino, H. Sieburg, R.A. Maki, E. Masliah, Myeloperoxidase polymorphism is associated with gender specific risk for Alzheimer's disease, *Exp. Neurol.* 155 (1999) 31–41.
- [23] Y. Sawayama, Y. Miyazaki, K. Ando, K. Horio, C. Tsutsumi, D. Imanishi, H. Tsushima, Y. Imaizumi, T. Hata, T. Fukushima, S. Yoshida, Y. Onimaru, M. Iwanaga, J. Taguchi, K. Kuriyama, M. Tomonaga, Expression of myeloperoxidase enhances the chemosensitivity of leukemia cells through the generation of reactive oxygen species and the nitration of protein, *Leukemia* 22 (2008) 956–964.
- [24] R.M. Nagra, B. Becher, W.W. Tourtellotte, J.P. Antel, D. Gold, T. Paladino, R.A. Smith, J.R. Nelson, W.F. Reynolds, Immunohistochemical and genetic evidence of myeloperoxidase involvement in multiple sclerosis, *J. Neuroimmunol.* 78 (1997) 97–107.
- [25] N.S. MacCallum, G.J. Quinlan, T.W. Evans, The Role of Neutrophil-Derived Myeloperoxidase in Organ Dysfunction and Sepsis, *Intensive care medicine*, Springer Berlin Heidelberg, 2007, pp. 173–187.
- [26] I.H. Buss, R. Senthilmohan, B.A. Darlow, N. Mogridge, A.J. Kettle, C.C. Winterbourn, 3-Chlorotyrosine as a marker of protein damage by myeloperoxidase in tracheal aspirates from preterm infants: association with

- adverse respiratory outcome, *Pediatr. Res.* 53 (2003) 455–462.
- [27] G.K. Hansson, A. Hermansson, The immune system in atherosclerosis, *Nat. Immunol.* 12 (2011) 204–212.
- [28] V. Rudolph, R.P. Andrie, T.K. Rudolph, K. Friedrichs, A. Klinke, B. Hirsch-Hoffmann, A.P. Schwoerer, D. Lau, X. Fu, K. Klingel, K. Sydow, M. Didie, A. Seniuk, E.C. von Leitner, K. Szoecks, J.W. Schrickel, H. Treede, U. Wenzel, T. Lewalter, G. Nickenig, W.H. Zimmermann, T. Meinertz, R.H. Boger, H. Reichenspurner, B.A. Freeman, T. Eschenhagen, H. Ehmkke, S.L. Hazen, S. Willems, S. Baldus, Myeloperoxidase acts as a profibrotic mediator of atrial fibrillation, *Nat. Med.* 16 (2010) 470–474.
- [29] S.J. Nicholls, S.L. Hazen, Myeloperoxidase and cardiovascular disease, *Arteriosclerosis, Thromb., Vasc. Biol.* 25 (2005) 1102–1111.
- [30] R.M. Roman, A.E. Wendland, C.A. Polanczyk, Myeloperoxidase and coronary arterial disease: from research to clinical practice, *Arq. Bras. Cardiol.* 91 (2008) e11–19.
- [31] A. Daugherty, J.L. Dunn, D.L. Rateri, J.W. Heinecke, Myeloperoxidase, a catalyst for lipoprotein oxidation, is expressed in human atherosclerotic lesions, *J. Clin. Invest.* 94 (1994) 437–444.
- [32] I. Aldib, J. Soubhye, K. Zouaoui Boudjeltia, M. Vanhaeverbeek, A. Rousseau, P.G. Furtmuller, C. Obinger, F. Dufrasne, J. Neve, P. Van Antwerpen, M. Prevost, Evaluation of new scaffolds of myeloperoxidase inhibitors by rational design combined with high-throughput virtual screening, *J. Med. Chem.* 55 (2012) 7208–7218.
- [33] E. Malle, G. Marsche, U. Panzenboeck, W. Sattler, Myeloperoxidase-mediated oxidation of high-density lipoproteins: fingerprints of newly recognized potential proatherogenic lipoproteins, *Arch. Biochem. Biophys.* 445 (2006) 245–255.
- [34] D. Steinberg, S. Parthasarathy, T.E. Carew, J.C. Khoo, J.L. Witztum, Beyond cholesterol, *N. Engl. J. Med.* 320 (1989) 915–924.
- [35] E. Malle, P.G. Furtmuller, W. Sattler, C. Obinger, Myeloperoxidase: a target for new drug development? *Br. J. Pharmacol.* 152 (2007) 838–854.
- [36] C.N. Theron, S. Lubbe, A. Van Zyl, Inhibitory effects of non-steroidal anti-inflammatory drugs on human myeloperoxidase, *South Afr. Med. J. = Suid Afrikaanse tydskrif vir geneeskunde* 56 (1979) 670–675.
- [37] G. Pekoe, K. Van Dyke, H. Mengoli, D. Peden, D. English, Comparison of the effects of antioxidant non-steroidal anti-inflammatory drugs against myeloperoxidase and hypochlorous acid luminol-enhanced chemiluminescence, *Agents Actions* 12 (1982) 232–238.
- [38] K.W. Zuurbier, A.R. Bakkenist, R.H. Fokkens, N.M. Nibbering, R. Wever, A.O. Muijsers, Interaction of myeloperoxidase with diclofenac. Inhibition of the chlorinating activity of myeloperoxidase by diclofenac and oxidation of diclofenac to dihydroxyazobenzene by myeloperoxidase, *Biochem. Pharmacol.* 40 (1990) 1801–1808.
- [39] W. Krol, Z. Czuba, S. Scheller, Z. Paradowski, J. Shani, Structure-activity relationship in the ability of flavonols to inhibit chemiluminescence, *J. Ethnopharmacol.* 41 (1994) 121–126.
- [40] M.L. Edwards, D.M. Stemerick, J.S. Sabol, K.A. Diekema, R.J. Dinerstein, Inhibition of myeloperoxidase release from rat polymorphonuclear leukocytes by a series of azachalcone derivatives, *J. Med. Chem.* 37 (1994) 4357–4362.
- [41] R.J.d.M. Albuquerque, L.K.A.M. Leal, M.A. Bandeira, G.S.d.B. Viana, L.V. Rodrigues, Chalcones from myracrodruon urundeuva are efficacious in Guinea pig ovalbumin-induced allergic conjunctivitis, *Rev. Bras. Farmacogn.* 21 (2011) 953–962.
- [42] M.L. Zeraik, V.F. Ximenes, L.O. Regasini, L.A. Dutra, D.H. Silva, L.M. Fonseca, D. Coelho, S.A. Machado, V.S. Bolzani, 4'-Aminochalcones as novel inhibitors of the chlorinating activity of myeloperoxidase, *Curr. Med. Chem.* 19 (2012) 5405–5413.
- [43] S. Kohnen, T. Franck, P. Van Antwerpen, K.Z. Boudjeltia, A. Mouthys-Mickalad, C. Deby, N. Moguilevsky, G. Deby-Dupont, M. Lamy, D. Serteyn, Resveratrol inhibits the activity of equine neutrophil myeloperoxidase by a direct interaction with the enzyme, *J. Agric. food Chem.* 55 (2007) 8080–8087.
- [44] Y. Kato, A. Nagao, J. Terao, T. Osawa, Inhibition of myeloperoxidase-catalyzed tyrosylation by phenolic antioxidants in vitro, *Biosci. Biotechnol. Biochem.* 67 (2003) 1136–1139.
- [45] J. Soubhye, I. Aldib, B. Elfving, M. Gelbcke, P.G. Furtmuller, M. Podrecca, R. Conotte, J.M. Colet, A. Rousseau, F. Reye, A. Sarakbi, M. Vanhaeverbeek, J.M. Kauffmann, C. Obinger, J. Neve, M. Prevost, K. Zouaoui Boudjeltia, F. Dufrasne, P. Van Antwerpen, Design, synthesis, and structure-activity relationship studies of novel 3-alkylindole derivatives as selective and highly potent myeloperoxidase inhibitors, *J. Med. Chem.* 56 (2013) 3943–3958.
- [46] J. Soubhye, M. Prevost, P. Van Antwerpen, K. Zouaoui Boudjeltia, A. Rousseau, P.G. Furtmuller, C. Obinger, M. Vanhaeverbeek, J. Ducobu, J. Neve, M. Gelbcke, F.O. Dufrasne, Structure-based design, synthesis, and pharmacological evaluation of 3-(aminoalkyl)-5-fluoroindoles as myeloperoxidase inhibitors, *J. Med. Chem.* 53 (2010) 8747–8759.
- [47] E.L. Thomas, M.B. Grisham, M.M. Jefferson, Myeloperoxidase-dependent effect of amines on functions of isolated neutrophils, *J. Clin. Invest.* 72 (1983) 441–454.
- [48] A.J. Kettle, C.A. Gedy, M.B. Hampton, C.C. Winterbourn, Inhibition of myeloperoxidase by benzoic acid hydrazides, *Biochem. J.* 308 (Pt 2) (1995) 559–563.
- [49] L.V. Forbes, P.G. Furtmuller, I. Khalilova, R. Turner, C. Obinger, A.J. Kettle, Isoniazid as a substrate and inhibitor of myeloperoxidase: identification of amine adducts and the influence of superoxide dismutase on their formation, *Biochem. Pharmacol.* 84 (2012) 949–960.
- [50] J.M. van Zyl, K. Basson, A. Kriegler, B.J. van der Walt, Mechanisms by which clofazimine and dapsone inhibit the myeloperoxidase system, *Biochem. Pharmacol.* 42 (1991) 599–608.
- [51] A. Boegevig, Y. Lo-Alfredsson, D. Pivonka, A.K. Tiden, Novel Pyrrolo[3,2-d]pyrimidin-4-one derivatives and Their Use in Therapy, Google Patents, 2006.
- [52] L.V. Forbes, T. Sjogren, F. Auchere, D.W. Jenkins, B. Thong, D. Loughton, P. Hemsley, G. Pairedeau, R. Turner, H. Eriksson, J.F. Unitt, A.J. Kettle, Potent reversible inhibition of myeloperoxidase by aromatic hydroxamates, *J. Biol. Chem.* 288 (2013) 36636–36647.
- [53] A. Roth, S. Ott, K.M. Farber, T.A. Palazzo, W.E. Conrad, M.J. Haddadin, D.J. Tantillo, C.E. Cross, J.P. Eiserich, M.J. Kurth, Inhibition of myeloperoxidase: evaluation of 2H-indazoles and 1H-indazolones, *Bioorg. Med. Chem.* 22 (2014) 6422–6429.
- [54] J. Zeng, R.E. Fenna, X-ray crystal structure of canine myeloperoxidase at 3 Å resolution, *J. Mol. Biol.* 226 (1992) 185–207.
- [55] T.J. Fiedler, C.A. Davey, R.E. Fenna, X-ray crystal structure and characterization of halide-binding sites of human myeloperoxidase at 1.8 Å resolution, *J. Biol. Chem.* 275 (2000) 11964–11971.
- [56] M. Blair-Johnson, T. Fiedler, R. Fenna, Human myeloperoxidase: structure of a cyanide complex and its interaction with bromide and thiocyanate substrates at 1.9 Å resolution, *Biochemistry* 40 (2001) 13990–13997.
- [57] X. Carpena, P. Vidossich, K. Schroetner, B.M. Calisto, S. Banerjee, J. Stamper, M. Soudi, P.G. Furtmuller, C. Rovira, I. Fita, C. Obinger, Essential role of proximal histidine-asparagine interaction in mammalian peroxidases, *J. Biol. Chem.* 284 (2009) 25929–25937.
- [58] A. Malvezzi, R.F. Queiroz, L. de Rezende, O. Augusto, A.T.d. Amaral, MPO inhibitors selected by virtual screening, *Mol. Inf.* 30 (2011) 605–613.
- [59] A.-K. Tidén, M. Svensson, A. Bernild, R. Senthilmohan, F. Auchère, H. Norman, P.-O. Markgren, S. Gustavsson, S. Schmidt, S. Lundquist, L.V. Forbes, N.J. Magon, L.N. Paton, G.N.L. Jameson, H. Eriksson, A.J. Kettle, 2-Thioxanthines are mechanism-based inactivators of myeloperoxidase that block oxidative stress during inflammation, *J. Biol. Chem.* 286 (2011) 37578–37589.
- [60] C.A. Davey, R.E. Fenna, 2.3 Å resolution X-ray crystal structure of the bisubstrate analogue inhibitor salicylhydroxamic acid bound to human myeloperoxidase: a model for a pre-reaction complex with hydrogen peroxide, *Biochemistry* 35 (1996) 10967–10973.
- [61] P. Van Antwerpen, M. Prevost, K. Zouaoui-Boudjeltia, S. Bazar, I. Legssyer, P. Moreau, N. Moguilevsky, M. Vanhaeverbeek, J. Ducobu, J. Neve, F. Dufrasne, Conception of myeloperoxidase inhibitors derived from flufenamic acid by computational docking and structure modification, *Bioorg. Med. Chem.* 16 (2008) 1702–1720.
- [62] G.E.K. Branch, The hydrolysis of hexahydropyrimidine, *J. Am. Chem. Soc.* 38 (1916) 2466–2474.
- [63] K. Robinson, A. McCluskey, M.I. Attalla, An ATR-FTIR study on the effect of molecular structural variations on the CO₂ absorption characteristics of heterocyclic amines, part II, *Chemphyschem a Eur. J. Chem. Phys. Phys. Chem.* 13 (2012) 2331–2341.
- [64] M. Hoffmann, J. Rychlewski, When, in the context of drug design, can a fluorine atom successfully substitute a hydroxyl group? *Int. J. Quantum Chem.* 89 (2002) 419–427.
- [65] R.F. Borch, M.D. Bernstein, H.D. Durst, Cyanohydrinborate anion as a selective reducing agent, *J. Am. Chem. Soc.* 93 (1971) 2897–2904.
- [66] A.F. Abdel-Magid, K.G. Carson, B.D. Harris, C.A. Maryanoff, R.D. Shah, Reductive amination of aldehydes and ketones with sodium triacetoxyborohydride. studies on direct and indirect reductive amination procedures(1), *J. Org. Chem.* 61 (1996) 3849–3862.
- [67] J.E. Wells, M.O. Browne, S. Aguilar-Gaxiola, A. Al-Hamzawi, J. Alonso, M.C. Angermeyer, C. Bouzan, R. Bruffaerts, B. Bunting, J.M. Caldas-de-Almeida, G. de Girolamo, R. de Graaf, S. Florescu, A. Fukao, O. Gureje, H.R. Hinkov, C. Hu, I. Hwang, E.G. Karam, S. Kostyuchenko, V. Kovess-Masfety, D. Levinson, Z. Liu, M.E. Medina-Mora, S.H. Nizamie, J. Posada-Villa, N.A. Sampson, D.J. Stein, M.C. Viana, R.C. Kessler, Drop out from out-patient mental healthcare in the world health organization's world mental health survey initiative, *Br. J. psychiatry J. Ment. Sci.* 202 (2013) 42–49.
- [68] M.J. Lim, C.A. Murray, T.A. Tronic, K.E. deKrafft, A.N. Ley, J.C. deButts, R.D. Pike, H. Lu, H.H. Patterson, Copper(I) cyanide networks: synthesis, structure, and luminescence behavior. Part 2. Piperazine ligands and hexamethylenetetramine(1), *Inorg. Chem.* 47 (2008) 6931–6947.
- [69] A. Bali, K. Sharma, A. Bhalla, S. Bala, D. Reddy, A. Singh, A. Kumar, Synthesis, evaluation and computational studies on a series of acetophenone based 1-(aryloxypropyl)-4-(chloroaryl) piperazines as potential atypical antipsychotics, *Eur. J. Med. Chem.* 45 (2010) 2656–2662.
- [70] G. Bernardinelli, D. Fernandez, R. Gosmini, P. Meier, A. Ripa, P. Schupfer, B. Treptow, E.P. Kundig, Alpha-t-butyl- and alpha-i-propyl-ortho-hydroxybenzylamines: racemic synthesis/resolution and asymmetric synthesis, *Chirality* 12 (2000) 529–539.
- [71] I. Ryu, H. Matsubara, S. Yasuda, H. Nakamura, D.P. Curran, Phase-vanishing reactions that use fluorous media as a phase screen. Facile, controlled bromination of alkenes by dibromine and dealkylation of aromatic ethers by boron tribromide, *J. Am. Chem. Soc.* 124 (2002) 12946–12947.
- [72] W. Jantschko, P.G. Furtmuller, M. Zederbauer, K. Neugschwandtner, I. Lehner, C. Jakopitsch, J. Arnhold, C. Obinger, Exploitation of the unusual thermodynamic properties of human myeloperoxidase in inhibitor design, *Biochem. Pharmacol.* 69 (2005) 1149–1157.

- [73] I.D. Tomlinson, H. Iwamoto, R.D. Blakely, S.J. Rosenthal, Biotin tethered homotryptamine derivatives: high affinity probes of the human serotonin transporter (hSERT), *Bioorg. Med. Chem. Lett.* 21 (2011) 1678–1682.
- [74] J. Arnhold, P.G. Furtmüller, C. Obinger, Redox properties of myeloperoxidase, *Redox Rep.* 8 (2003) 179–186.
- [75] P.G. Furtmuller, J. Arnhold, W. Jantschko, H. Pichler, C. Obinger, Redox properties of the couples compound I/compound II and compound II/native enzyme of human myeloperoxidase, *Biochem. Biophys. Res. Commun.* 301 (2003) 551–557.
- [76] G. Battistuzzi, M. Bellei, M. Zederbauer, P.G. Furtmuller, M. Sola, C. Obinger, Redox thermodynamics of the Fe(III)/Fe(II) couple of human myeloperoxidase in its high-spin and low-spin forms, *Biochemistry* 45 (2006) 12750–12755.
- [77] J. Arnhold, P.G. Furtmuller, C. Obinger, Redox properties of myeloperoxidase, *Redox Rep. Commun. free Radic. Res.* 8 (2003) 179–186.
- [78] A.J. Kettle, C.C. Winterbourn, Mechanism of inhibition of myeloperoxidase by anti-inflammatory drugs, *Biochem. Pharmacol.* 41 (1991) 1485–1492.
- [79] J. Sadowski, J. Gasteiger, From atoms and bonds to three-dimensional atomic coordinates: automatic model builders, *Chem. Rev.* 93 (1993) 2567–2581.
- [80] R.A. Friesner, J.L. Banks, R.B. Murphy, T.A. Halgren, J.J. Klicic, D.T. Mainz, M.P. Repasky, E.H. Knoll, M. Shelley, J.K. Perry, D.E. Shaw, P. Francis, P.S. Shenkin, Glide: a new approach for rapid, accurate docking and scoring. 1. Method and assessment of docking accuracy, *J. Med. Chem.* 47 (2004) 1739–1749.
- [81] J. Shelley, A. Cholleti, L. Frye, J. Greenwood, M. Timlin, M. Uchimaya, Epik: a software program for pK_a prediction and protonation state generation for drug-like molecules, *J. Comput. Aided Mol. Des.* 21 (2007) 681–691.
- [82] P. Van Antwerpen, P. Moreau, K. Zouaoui Boudjeltia, S. Babar, F. Dufrasne, N. Moguilevsky, M. Vanhaeverbeek, J. Ducobu, J. Neve, Development and validation of a screening procedure for the assessment of inhibition using a recombinant enzyme, *Talanta* 75 (2008) 503–510.
- [83] P.G. Furtmuller, W. Jantschko, G. Regelsberger, C. Jakopitsch, J. Arnhold, C. Obinger, Reaction of lactoperoxidase compound I with halides and thiocyanate, *Biochemistry* 41 (2002) 11895–11900.
- [84] D.P. Nelson, L.A. Kiesow, Enthalpy of decomposition of hydrogen peroxide by catalase at 25° C (with molar extinction coefficients of H₂O₂ solutions in the UV), *Anal. Biochem.* 49 (1972) 474–478.
- [85] P.G. Furtmuller, U. Burner, C. Obinger, Reaction of myeloperoxidase compound I with chloride, bromide, iodide, and thiocyanate, *Biochemistry* 37 (1998) 17923–17930.
- [86] A.S. Kristensen, M.B. Larsen, L.B. Johnsen, O. Wiborg, Mutational scanning of the human serotonin transporter reveals fast translocating serotonin transporter mutants, *Eur. J. Neurosci.* 19 (2004) 1513–1523.
- [87] M.B. Larsen, B. Elfving, O. Wiborg, The chicken serotonin transporter discriminates between serotonin-selective reuptake inhibitors. A species-scanning mutagenesis study, *J. Biol. Chem.* 279 (2004) 42147–42156.
- [88] R.G. Parr, W. Yang, Density functional approach to the frontier-electron theory of chemical reactivity, *J. Am. Chem. Soc.* 106 (1984) 4049–4050.
- [89] P. Geerlings, F. De Proft, W. Langenaeker, Conceptual density functional theory, *Chem. Rev.* 103 (2003) 1793–1873.
- [90] G.W.T.M.J. Frisch, H.B. Schlegel, G.E. Scuseria, M.A. Robb, J.R. Cheeseman, G. Scalmani, V. Barone, B. Mennucci, G.A. Petersson, H. Nakatsuji, M. Caricato, X. Li, H.P. Hratchian, A.F. Izmaylov, J. Bloino, G. Zheng, J.L. Sonnenberg, M. Hada, M. Ehara, K. Toyota, R. Fukuda, J. Hasegawa, M. Ishida, T. Nakajima, Y. Honda, O. Kitao, H. Nakai, T. Vreven, J.A. Montgomery Jr., J.E. Peralta, F. Ogliaro, M. Bearpark, J.J. Heyd, E. Brothers, K.N. Kudin, V.N. Staroverov, R. Kobayashi, J. Normand, K. Raghavachari, A. Rendell, J.C. Burant, S.S. Iyengar, J. Tomasi, M. Cossi, N. Rega, J.M. Millam, M. Klene, J.E. Knox, J.B. Cross, V. Bakken, C. Adamo, J. Jaramillo, R. Gomperts, R.E. Stratmann, O. Yazyev, A.J. Austin, R. Cammi, C. Pomelli, J.W. Ochterski, R.L. Martin, K. Morokuma, V.G. Zakrzewski, G.A. Voth, P. Salvador, J.J. Dannenberg, S. Dapprich, A.D. Daniels, Ö. Farkas, J.B. Foresman, J.V. Ortiz, J. Cioslowski, D.J. Fox, Gaussian 09, Revision A.01, Wallingford CT, 2009.